Energy Conversion and Management: X 27 (2025) 101209

Contents lists available at ScienceDirect

Energy Conversion and Management: X

journal homepage: www.sciencedirect.com/journal/energy-conversion-and-management-x

Optimizing a hybrid off-grid photovoltaic/wind/fuel cell energy system using mantis search algorithm

Saleh Awadh AL Dawsari [a,b,*], Fatih Anayi [a], Michael Packianather [a]

[a] School of Engineering, Cardiff University, Cardiff CF24 3AA, UK
[b] Electrical Engineering Department, College of Engineering, Najran University, Najran, Saudi Arabia

ARTICLE INFO

Keywords:
MSA optimization technique
PV
Wind
Fuel Cell
Electrolyzer
Energy

ABSTRACT

The rising global demand for environmentally friendly energy sources calls for the development of effective hybrid renewable power plants. This work addresses the design and operation optimization of an off-grid PV/Wind/Fuel cell system to meet energy needs in the Najran area of Saudi Arabia, with plenty of renewable resources. The mantis search algorithm (MSA) can effectively lower the cost of energy (COE) while preserving system dependability considering its superior convergence characteristics based on the foraging and mating activities of praying mantises. Using the loss of power supply probability (LPSP) as the reliability metric, the MSA algorithm was applied on two system configurations to optimizing the capacities of photovoltaic panels, wind turbines, fuel cells, electrolyzers, and hydrogen tanks. The analysis of the cost of energy (COE) and loss of power supply probability (LPSP) for the PV/Wind/FC and PV/FC configurations, based on four cases each with various objective functions, shows that the PV/Wind/FC system generally provides a lower COE and LPSP compared to the PV/FC system. For the PV/Wind/FC system, COE ranges from 0.161154 US$/kWh to 0.237477 US$/kWh, and LPSP ranges from 0.022517 % to 0.057322 %. In contrast, the PV/FC system shows higher COE values, ranging from 0.380493 US$/kWh to 0.500352 US$/kWh, with LPSP values ranging from 0.036985 % to 0.099117 %. Moreover, Statistical analysis of results from various system configurations confirms the accuracy and stability of the MSA algorithm. The findings demonstrate that MSA effectively achieves optimal system design while ensuring acceptable energy fluctuation and efficient use of renewable resources. The Break-Even Grid Extension Distance (BED) analysis for the PV/Wind/FC and PV/FC configurations shows that the PV/Wind/FC system is more cost-effective for off-grid solutions over shorter distances, with the PV/FC system providing a more favorable option for longer distances, where the break-even distance for the PV/Wind/FC system ranges from 18.21 km to 143.66 km and for the PV/FC system from 376.41 km to 572.14 km.

1. Introduction

1.1. Motivation and background

The world is seeing a growing trend toward the use of renewable energy sources, particularly solar and wind power, in electric utility operations [1,2]. However, the integration of large amounts of variable renewable energy generation poses various challenges [3,4]. These challenges include navigating uncertain weather conditions, coping with fluctuations in consumer demand, addressing the mismatch between demand and variable generation, and dealing with technical system constraints, regulatory policy requirements, and economic cost

Abbreviations: BAT, Battery; COE, Cost of Energy; COH, Cost of Hydrogen; BED, Break-Even Grid Extension Distance; DG, Diesel Generator; GA, Genetic Algorithm; GHI, Global Horizontal Irradiance; GWO, Grey Wolf Optimizer; HES, Hybrid Energy System; HOMER, Hybrid Optimization Model for Multiple Energy Resources; HRES, Hybrid Renewable Energy System; kWh, Kilowatt-hour; LCOE, Levelized Cost of Energy; LPSP, Loss of Power Supply Probability; LCOH, Levelized Cost of Hydrogen; LF-SSA, Lévy Flight Salp Swarm Algorithm; LPM, Linear Programming Model; MILP, Mixed-Integer Linear Programming; MOPSO, Multi-Objective Particle Swarm Optimization; MSA, Mantis Search Algorithm; NPC, Net Present Cost; NSGA-II, Non-Dominated Sorting Genetic Algorithm II; PHES, Pumped-Hydro Energy Storage; PRISMA, Preferred Reporting Items for Systematic Reviews and Meta-Analyses; PSO, Particle Swarm Optimization; PV, Photovoltaic; RF, Renewable Fraction; TES, Thermal Energy Storage; TLBO, Teaching-Learning-Based Optimization; USD, United States Dollar; WT, Wind Turbine; CSA, Cuckoo Search Algorithm; COH, Cost Of Hydrogen; LCOH, Levelized Cost Of Hydrogen; PHES, Pumped-Hydro Storage; NFL, No Free Lunch.

* Corresponding author.
E-mail addresses: Aldawsarisa@cardiff.ac.uk (S.A. AL Dawsari), anayi@cardiff.ac.uk (F. Anayi), packianatherms@cardiff.ac.uk (M. Packianather).

https://doi.org/10.1016/j.ecmx.2025.101209
Received 30 December 2024; Received in revised form 4 August 2025; Accepted 15 August 2025
Available online 18 August 2025

considerations [5,6]. In simple terms, batteries play a vital role in hybrid power systems in remote areas [6,7]. Accurate prediction of battery lifetime and analysis of battery performance over time is important for designing efficient and cost-effective renewable energy storage systems [8]. Researchers have suggested methods for assessing total operating costs and identifying optimal designs for microgrid hybrid power systems with energy storage, thereby helping to make these systems more effective and economical [9,10].

1.2. Literature review

Researchers often use different strategies when it comes to determining the appropriate size for hybrid renewable energy systems (HRES) [11]. The reviewed studies thoroughly examined the available literature, used software tools, applied traditional methodologies, and investigated metaheuristic approaches [12,13,14,15]. Among the software tools commonly employed in this domain, the hybrid optimization model for multiple energy resources (HOMER) stands out as a popular choice. It aids in the unit sizing process for HRES by providing a comprehensive and efficient platform for analyzing multiple energy resources [16]. In [17], researchers examined the applicability of HRES in Kallar Kahar, Punjab, Pakistan. HOMER software was used to analyze the WT, PV, and biomass installations. The research found that Kallar Kahar has excellent potential for HRES energy generation, owing to its sun irradiation, wind, and animal manure. The estimated price of implementing the HRES to meet the 73.6 MW peak demand was 180.2 million US dollars. This article examines whether a mini-grid renewable energy system can power Kibran Gabriel Island in Ethiopia. Research [18] compared a mini-grid system with diesel generation and grid expansion systems using HOMER Pro simulation, optimization, and sensitivity analysis. The hybrid photovoltaic (PV)/DG/battery system was the most cost-effective, with a COE of USD 0.175/kWh, NPC of USD 119,139, and RF of 86.4 %. This technology decreases pollutant emissions by 33,102 kg/yr compared with diesel generation alone. According to the sensitivity analysis, the system works effectively with fluctuations in global horizontal irradiance (GHI), diesel prices, and load consumption.

The classical method employs differential calculus as a tool for optimizing solutions [15,19,20]. This method utilizes mathematical techniques to ascertain the optimal outcome or approach to a given problem [21]. Given the limited effectiveness of classical methods in optimizing spatial resources, researchers have not frequently utilized these techniques [22,23]. However, academic discourse has acknowledged and explored several classical optimization approaches, such as the linear programming (LPM) model [24]. To determine the optimal size for HRESs, the present study introduces the mixed-integer linear programming (MILP) optimization algorithm. The MILP algorithm was tested in a real-world case involving a mountain hut in South Tyrol. The optimization approach considered different configurations using solar panels, wind turbines, and diesel generators. This MILP-based tool supports engineering decisions by identifying the most cost-effective and energy-efficient configuration during the planning stage of a hybrid renewable energy system [25].

Metaheuristic problem-solving methodologies have recently emerged [26,27,28]. In [29], researchers attempted various optimization techniques, such as ant colony optimization, firefly algorithm, particle swarm optimization (PSO), and genetic algorithm (GA). They found that PSO outperformed the other methods in optimizing the levelized cost of energy (LCOE). Another investigation [30] determined the optimal size of a hybrid energy system (HES) using a Social Spider optimizer. Moving on to a different research paper [12], it was found that the harmony search algorithm outperformed PSO and Jaya in optimizing a PV-WT-biomass-BAT system. The primary aim was to enhance the efficiency of this system in terms of renewable energy, cost-effectiveness, and reliability, all of which meet consumers' energy needs. Furthermore, Ref. [31] utilized the salp swarm algorithm to optimize the LCOE, considering various combinations of three types of batteries. Moreover, a systematic review has examined the progress with HRES optimization using software-driven, hybrid, AI-based, and classical methods [32]. The research in [33] explores optimization strategies that balance economic, environmental, social, and technical criteria using algorithms including MOPSO, NSGA-II, CSA, GWO, LF-SSA, and MILP in conjunction with tools including HOMER Pro and MATLAB. Examining 138 research papers from Scopus that investigate renewable energy system optimization over the past 24 years [34] using the PRISMA framework and bibliophagy.

Moreover, Table 1 introduces a review of the research effort to confirm the diversity of the applied methods as well as the variety of suggested microgrid configurations [35 36 37 5 8 38 39 40 11 41]. The key observations from the comparative analysis of the studies reveal several critical insights. First, PV/Wind/Battery systems consistently emerge as the most cost-effective configuration across multiple studies, with the cost of energy (COE) ranging from $0.151/kWh to $0.8056/kWh [39 11 41]. However, Koholé et al. [37] highlight the PV/Wind/Fuel Cell system as the most efficient for energy production, achieving a COE as low as $0.94/kWh for multimedia facilities in Maroua. Second, optimization methods such as the Cuckoo Search Algorithm (CSA) and Teaching-Learning-Based Optimization (TLBO) are frequently employed and demonstrate superior performance in designing and optimizing hybrid renewable energy systems, ensuring cost efficiency and reliability [35 5 39 11]. Third, these systems offer significant environmental benefits, with reductions in CO2 emissions of up to 98.79 % in some cases, contributing to global efforts to combat climate change [35 36 40 41]. Fourth, wind energy systems show considerable promise for hydrogen production, with the cost of hydrogen (COH) as low as $4.3865/kg in Kousseri [38]. Koholé et al. [37] further highlight the photovoltaic/fuel cell system as the most cost-effective for hydrogen production, achieving a levelized cost of hydrogen (LCOH) of $8.91/kg for multimedia facilities in Mbouda. Finally, systems incorporating thermal energy storage (TES) and pumped-hydro storage (PHES) are noted for TES and PHES systems' reliability and environmental advantages, further enhancing the value of such technologies for sustainable energy solutions [35 5 40]. Overall, existing studies provide a comprehensive framework for optimizing hybrid renewable energy systems, emphasizing the systems' contributions to cost-effectiveness, reliability, and sustainability.

Researchers in [42 43 3 44 45] demonstrate the techno-economic and environmental potential of hybrid renewable energy systems for hydrogen generation and storage. Ref. [42] highlights the performance of hybrid PV/Wind systems in different locations, with Mersa Matruh producing 118,115 kWh/year of electricity and 1,972 kg/year of hydrogen, Aswan generating 107,285 kWh/year and 1,795 kg/year of hydrogen, and Cairo producing 84,096 kWh/year and 1,418 kg/year of hydrogen. The levelized cost of hydrogen (LCOH) in this study ranged from $4.54/kg to $7.48/kg, indicating competitive hydrogen production costs. Ref. [43] focuses on large-scale hydrogen generation, showing that Dakhla, Morocco, achieved the lowest LCOH of $2.54/kg through an optimized combination of solar arrays and wind farms. Ref. [3] emphasizes the efficiency of PV/Wind/Diesel/Battery/Electrolyzer systems for co-generating electricity and hydrogen, achieving an optimal ecological footprint with a cost of electricity at $0.252/kWh and a cost of hydrogen at $2.59/kg. Ref. [44] explores the scalability of renewable energy systems, with a 100 MW PV system producing 158,484–175,675 MWh/year of electricity and 2,524–2,761 tonnes/year of hydrogen, achieving an LCOH of 22.54–28.38 CNY/kg and an energy efficiency of 9.03–9.31 %. Finally, Ref. [45] showcases the environmental and economic benefits of a hydrogen-methane thermal power plant, which achieved a 16-year payback period with 100 % hydrogen combustion and an annual CO2 reduction of 155 tones. Ourya et al. (2023) [43] conducted a techno-economic analysis of large-scale hydrogen production using hybrid PV/Wind systems in Morocco, identifying Dakhla as the most cost-effective location with a levelized cost of

Table 1
A review of research effort to confirm the diversity of the applied methods and platforms as well as the variety of suggested microgrid configurations.

Ref.	Focus	Technologies Evaluated	Optimization Method	Key Findings	Cost Metrics
Ref. [35]	Comparison of battery, hydrogen, pumped-hydro, and thermal energy storage technologies	PV, Wind, Battery, Fuel Cell, Pumped-Hydro, Thermal Energy Storage (TES)	Cuckoo Search Algorithm (CSA)	PV/Wind/TES system most cost-effective; COE: $0.2100/kWh (heavy activity); TES outperforms other storage technologies in cost and reliability.	COE: $0.2100–$0.2277/kWh
Ref. [36]	Optimization of hybrid PV/Wind/Diesel/Fuel Cell systems for residential applications	PV, Wind, Diesel, Fuel Cell	Evolutionary Algorithms	PV/Wind/Diesel/FC system was the most cost-effective; COE: $1.087/kWh (high demand); CO2 emissions: 1504.2 kg/year (low demand).	COE: $1.087–$2.384/kWh
Ref. [37]	Green hydrogen production and storage via hybrid systems	PV, Wind, Fuel Cell, Electrolyzer, Hydrogen Tank	Teaching-Learning-Based Optimization (TLBO)	PV/Wind/Fuel Cell system most efficient for energy production; COE: $0.94/kWh (Maroua); COH: $8.91/kg (Mbouda).	COE: $0.94–$1.93/kWh; COH: $8.91–$24.61/kg
Ref. [5]	Optimization of hybrid PV/Wind systems with thermal and pumped-hydro storage	PV, Wind, Thermal Energy Storage (TES), Pumped-Hydro Energy Storage (PHES)	Cuckoo Search Algorithm (CSA)	PV/Wind/TES most cost-effective; Wind/PHES most reliable and eco-friendly; significant CO2 emission reductions.	COE: $0.2100–$0.2641/kWh
Ref. [8]	Hybrid PV/Wind/Battery/Diesel systems for rural electrification	PV, Wind, Battery, Diesel	Teaching-Learning-Based Optimization (TLBO)	PV/Wind/Battery/Diesel system most cost-effective; COE: $0.2158/kWh (healthcare center); break-even grid extension distance: 0.443 km (household).	COE: $0.2158–$0.2419/kWh
Ref. [38]	Wind energy potential for electricity and hydrogen production	Wind Turbines, Electrolyzer, Hydrogen Storage	None (Techno-economic analysis)	Kousseri is best for hydrogen production; COE: $0.0578/kWh; COH: $4.3865/kg (GE 1.5SL turbine); payback period: 2.9 years (Enercon E-48/800).	COE: $0.0578–$0.0838/kWh; COH: $4.3865–$6.5065/kg
Ref. [39]	Quantitative techno-economic comparison of PV/Wind systems with various storage technologies	PV, Wind, Battery, Fuel Cell	Cuckoo Search Algorithm (CSA)	PV/Wind/Battery system most cost-effective; COE: $0.1570/kWh (heavy activity, Fotokol); PV/Wind/Fuel Cell system viable but higher cost.	COE: $0.1570–$0.8056/kWh
Ref. [40]	Techno-economic analysis of hybrid PV/Wind/Diesel systems with multiple storage technologies	PV, Wind, Diesel, Battery, Pumped-Hydro, Hydrogen, Thermal Energy Storage (TES)	Cuckoo Search Algorithm (CSA)	PV/Wind/Diesel/TES system is the most cost-effective; COE: $0.2461/kWh; CO2 emissions reduced by up to 98.79 % compared to diesel-only systems.	COE: $0.2461–$0.2649/kWh
Ref. [11]	Techno-economic analysis of standalone PV/Wind hybrid systems with battery and fuel cell	PV, Wind, Battery, Fuel Cell	Cuckoo Search Algorithm (CSA)	PV/Wind/Battery system most cost-effective; COE: $0.1959/kWh (heavy activity); superior performance of CSA in optimizing system design.	COE: $0.1959–$0.2641/kWh
Ref. [41]	Techno-economic and environmental assessment of hybrid PV/Wind/Diesel systems	PV, Wind, Diesel, Battery, Fuel Cell	Cuckoo Search Algorithm (CSA)	PV/Wind/Battery/Diesel system most cost-effective; COE: $0.151/kWh (Idabato); CO2 emissions reduced by 94.32 % for high consumers.	COE: $0.151–$0.220/kWh
Ref. [42]	Techno-economic analysis of hybrid PV/Wind systems for hydrogen generation and storage	PV, Wind, Electrolyzer, Hydrogen Storage	A transient mathematical model using MATLAB/Simulink	Mersa Matruh produced 118,115 kWh/year and 1,972 kg/year of hydrogen; Aswan produced 107,285 kWh/year and 1,795 kg/year of hydrogen; Cairo produced 84,096 kWh/year and 1,418 kg/year of hydrogen.	The levelized cost of hydrogen (LOCH) ranges from 4.54 $/kg to 7.48 $/kg
Ref. [43]	Techno-economic study of large-scale hydrogen generation via hybrid PV/Wind systems	PV, Wind, Electrolyzer, Hydrogen Storage	Optimization of PV/Wind ratio	Dakhla, Morocco, achieved the lowest LCOH of $2.54/kg using a combination of solar arrays and wind farms.	LCOH: $2.54/kg
Ref. [3]	Techno-economic and environmental assessment of PV/Wind/Diesel/Battery/Electrolyzer systems	PV, Wind, Diesel, Battery, Electrolyzer	Multi-criteria decision-making	PV/Wind/Diesel/Battery/Electrolyzer system most efficient for co-generation of electricity and hydrogen; achieved optimal ecological footprint and lowest hydrogen production cost.	cost of electricity-$ 0.252/kWh, cost of hydrogen-$ 2.59/kg,
Ref. [44]	Computational strategy for 100 MW PV system coupled to hydrogen generation	PV, Electrolyzer, Hydrogen Storage	Process Modeling based MATLAB	System produced 158,484–175,675 MWh/year of electricity and 2,524–2,761 tonnes/year of hydrogen; LCOH: 22.54–28.38 CNY/kg; energy efficiency: 9.03–9.31 %.	LCOH: 22.54–28.38 CNY/kg
Ref. [45]	Hydrogen-methane thermal power plant for a high school	PV, Electrolyzer, Hydrogen Storage	ON/OFF control	The system achieved a 16-year payback period with 100 % hydrogen combustion; an annual CO2 reduction of 155 tonnes.	N/A
Ref. [46]	Hydrogen-methane thermal power plant for a high school	PV, Electrolyzer, Hydrogen Storage	HOMER Pro	The system achieved a 16-year payback period with 100 % hydrogen combustion; an annual CO2 reduction of 155 tones.	LCOH: 2.54$/kg

hydrogen (LCOH) of $2.54/kg. Their findings highlight the potential of combining photovoltaic panels and wind turbines for low-cost hydrogen production, emphasizing that the cost of water desalination is negligible, representing only 0.12 % to 0.35 % of the net present costs.

Mutually, the presented literature studies illustrate the significant potential of hybrid renewable energy systems for sustainable hydrogen production, cost-effectiveness, and environmental impact reduction. It is notable that metaheuristic algorithms possess inherent limitations primarily due to the challenge of balancing exploration and exploitation, which directly impacts algorithmic performance. Moreover, parameter selection is crucial for optimizing efficiency; however, identifying the optimal parameters is difficult. Novel methods lacking parameter sensitivity and qualitative analysis may struggle to address complex problems. Certain algorithms rank conceptual novelty over computational efficiency, leading to suboptimal performance for various problem types. The No Free Lunch (NFL) theorem emphasizes the necessity of enhancing existing techniques or developing novel approaches, as it demonstrates that no singular method can optimally address all optimization problems [46].

1.3. Research gap

As introduced, while much research gives attention to the optimal design of the hybrid renewable energy systems (HRES), the optimization of off-grid systems—particularly in areas with plenty of renewable resources like Najran—remains underactive. The difficulty of creating an effective off-grid PV/Wind/Fuel Cell system that can consistently satisfy energy needs while minimizing costs is addressed by this work.

Metaheuristic algorithms are essential for optimization but have certain limitations: (i) Balancing exploration and exploitation phases is challenging but critical for overall performance. (ii) The performance of most algorithms is heavily influenced by parameters, and determining optimal parameters for specific problems is difficult. Without addressing parameter sensitivity, algorithms may struggle with complex issues. (iii) Some algorithms focus on novel metaphors without improving computational performance, leading to inefficiency and suboptimal results. The No Free Lunch (NFL) theorem suggests no single algorithm excels at all optimization problems, highlighting the need for adapting or creating new methods. Moreover, MSA is reported as a promising recent metaheuristic algorithm that has proven effective in addressing complex, nonlinear, and optimization challenges. Its unique approach integrates both exploration and exploitation phases, allowing it to strike a balance between the global search for optimal solutions and avoidance of local minima. This capability is particularly important for systems with nonlinear constraints, such as those met in energy and resource management.

Although conventional metaheuristic methods including PSO and GA and other reported works have been extensively applied for HRES optimization, To the best of the authors' knowledge, the Mantis Search Algorithm (MSA) has not been thoroughly investigated in this context. This work closes this gap by proving MSA's better convergence properties in system configuration optimization, so guaranteeing both system reliability and economy. This study assesses several system designs and shows the ability of the MSA algorithm to minimize the cost of energy (COE) while keeping an acceptable loss of power supply probability (LPSP), so achieving an optimal cost-reliability balance. Furthermore sometimes disregarded in research on renewable energy is statistical validation of optimization results. Employing a thorough statistical analysis of system configurations, this work validates the stability and accuracy of the MSA algorithm. The results confirm MSA's capacity to keep constant performance under different environments. Although off-grid uses of hydrogen-based energy storage systems are under increasing consideration, their optimization inside HRES is still under insufficient research. Especially pertinent for arid areas with great solar and wind potential, this study offers insights into the effective integration of hydrogen storage by including electrolyzers and hydrogen tanks in the optimization process.

1.4. Contribution and paper organization

This paper introduces the application of the MSA optimization algorithm for the optimal design of various configuration models within a hybrid off-grid energy system proposed for Najran, KSA. The developed algorithm aims to minimize the COE generated by the suggested models over their presumed lifetime. Additionally, minimizing the LPSP is a primary objective for the developed algorithm. The algorithm is tested on two distinct configurations of a hybrid off-grid energy system to evaluate its effectiveness. Statistical measures are subsequently presented to assess the reliability and efficiency of the developed algorithm. The MSA algorithm stands out as a competitive alternative to existing metaheuristic algorithms due to several key advantages. It is straightforward to implement and effectively maintains population diversity throughout the optimization process. The algorithm demonstrates a strong capability to avoid local optima and includes a robust exploitation operator, enabling it to handle unimodal functions efficiently. Additionally, MSA achieves an optimal balance between exploration and exploitation by dynamically switching between searching for prey and attacking prey.

The subsequent sections of this paper are organized as follows: Section II delves into the System configuration and sizing formulation. Section III elucidates the operating strategy employed in the proposed hybrid system, followed by Section IV, which outlines the optimization algorithm. Section V provides a comprehensive presentation of the obtained results and ensuing discussions. Finally, Section VI offers a summarized conclusion of the work.

2. System configuration and sizing formulation

This study focuses on the residential area in Najran, KSA. As shown in Fig. 1, the proposed HRES uses wind turbines and solar panels to meet consumer demand. A combination of fuel cells, electrolyzers, and hydrogen fuel tanks was employed for energy storage to ensure reliability. This setup is considered a "green" system with environmentally friendly energy resources. Excess PV-WT energy triggers hydrogen production by the electrolyzer, whereas fuel cells provide energy when renewable sources fall short. The hybrid (AC–DC) bus structure simplifies the model, featuring inverters and converters. Due to oxidation effects from the acidic content in water, desalination must be implemented before introducing water into the electrolyzer to prevent component degradation. The cost of desalination is negligible compared to overall system expenses, making it a viable addition without significantly affecting economic feasibility [43]. This process is essential for optimizing hydrogen production and ensuring the reliability of hybrid renewable energy systems. While desalination was assumed negligible in this study, its necessity depends on the water source.

2.1. PV system model

Getting detailed information about the amount of sunlight reaching the solar panels every hour is crucial for planning the hybrid system effectively. To accurately calculate the power output of each photovoltaic panel in relation to the available solar radiation, you can use equation (1) [47]:

$$P_{PV}(t) = P_{R,PV} \times \left(R/R_{ref}\right) \times \left[1 + N_T\left(T_c - T_{ref}\right)\right] \quad (1)$$

The amount of power a single solar panel produces at a specific time, labeled as $P_{\mathrm{PV}}(t)$, is figured out using equation (1), t. $P_{R,\mathrm{PV}}$ stands for the panel's rated power. R represents solar radiation, measured in watts per square meter (W/m^2), and R_{ref} is the standard radiation, usually set at 1000 W/m^2. T_{ref} is the cell's temperature under standard conditions, typically at 25$^{\circ}C$. There's a temperature coefficient called "NT," set at

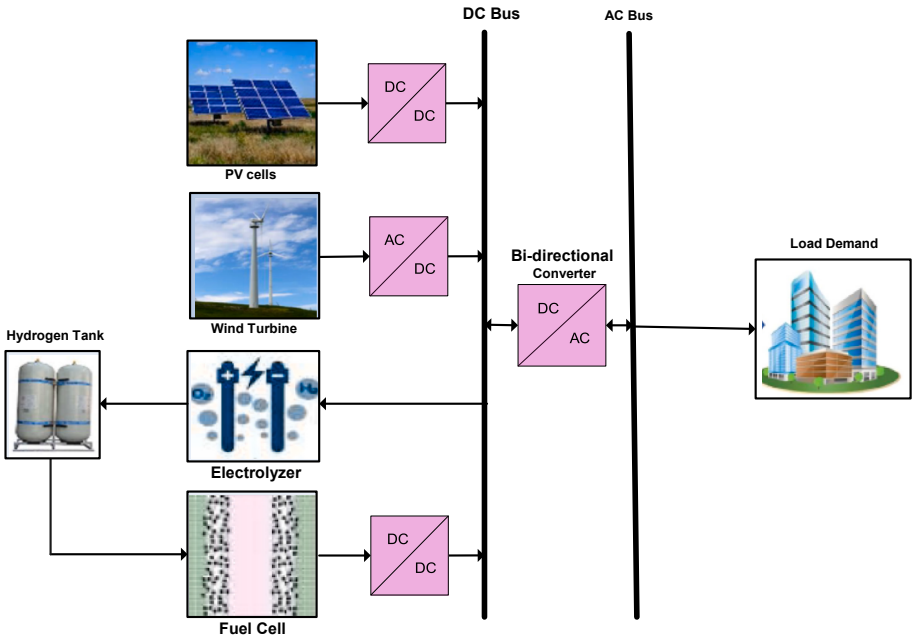

Fig. 1. Conceptual illustration of the proposed renewable energy hybrid PV-Wind-FC system.

−3.7 x 10–3 per degree Celsius (°C), applicable to both mono and polycrystalline silicon types. Equation (2) helps calculate the actual cell temperature, denoted as T_c.

$$T_c = T_{\text{air}} + (((\text{NOCT} - 20)/800) \times R_a) \tag{2}$$

The air temperature, denoted as T_{air}, is in degrees Celsius, and R_a represents radiation. Also, there's something called "NOCT," which stands for the operating cell temperature, measured in degrees Celsius. Manufacturers provide these important details for photovoltaic (PV) modules. Now, if we have a bunch of PV systems, let's define that. N_{PV}, the total power they generate at a specific time is $P_{\text{PV}}(t)$, can be calculated $P_{\text{PV}}(t) = N_{\text{PV}} \times p_{\text{PV}}(t)$.

2.2. Wind turbine (WT) system model

Wind power is seen as a really promising type of energy. One cool thing about it is that it doesn't produce greenhouse gas emissions, making it environmentally friendly. Plus, it's economically efficient, which makes people like it even more. We use a wind turbine with several blades connected to a generator to harness wind energy. This setup captures the wind's energy, and the turbine is placed on a high structure to do this effectively. We can figure out how much power each wind turbine produces using a specific equation (3) [48,49]:

$$\begin{cases} P_{WT}(t) = 0 & V(t) < V_{IN} \\ P_{WT}(t) = a(V(t))^3 - bP_R & V_{IN} < V(t) < V_R \\ P_{WT}(t) = P_R & V_R < V(t) < V_{UP} \\ P_{WT}(t) = 0 & V(t) > V_{UP} \end{cases} \tag{3}$$

The values for a and b are found by using equation (4).

$$\begin{cases} a = \dfrac{P_{R,WT}}{V_R^3 - V_{IN}^3} \\ b = \dfrac{V_{IN}^3}{V_R^3 - V_{IN}^3} \end{cases} \tag{4(}$$

Expressing the overall power generated can be done as:

$$P_R = \frac{1}{2} A_{WT} \cdot C_P \cdot \rho_a \cdot \eta_{WT} \cdot V_R^3 \tag{5}$$

The power produced by individual wind turbines at a specific time is denoted by $P_{WT}(t)$. The nominal power of a wind turbine is represented as $P_{R,\text{WT}}$, and the wind speed is indicated by V. V_{IN} stands for the speed triggering the low cut, while V_{UP} is the speed causing the up cut. Also, V_R is the speed linked to the nominal power. The swept area of the wind turbines is represented as A_{WT}, and η_{WT} is the efficiency of the wind turbine. The power coefficient, labeled as C_P, and the air density, denoted by ρ_a.

Equation (3) defines wind turbine efficiency based on its output characteristics and wind velocity (V). Power production P_{WT} is zero when wind velocity is below the cut-in speed V_{IN} or exceeds the cut-off speed V_{UP}. Within the range between cut-in and rated wind velocity V_R, power generation follows a nonlinear increase. When wind velocity falls between the rated and threshold speeds, the turbine maintains a constant power output at its rated capacity.

2.3. Modelling electrolyzers

The surplus energy produced by solar panels (PVs) and wind turbines is employed to power the electrolyzer. This device is responsible for producing hydrogen by splitting water into oxygen (at the cathode) and hydrogen (at the anode) through the application of a direct current (DC) across two electrodes (refer to Equation (6)) [50]. Subsequently, the generated hydrogen is stored in high-pressure tanks [51].

$$\text{Electricity} + \text{H}_2\text{O} = \text{H}_2 + \frac{1}{2}\text{O}_2 \tag{6}$$

The illustration outlines the process of the electrolyzer directing energy to the hydrogen storage tank, as explicitly stated in the equation (7) [50].

$$\text{P}_{\text{ele}-\text{H}_2\text{t}} = \text{P}_{\text{ren}_{\text{ele}}} \times \eta_{\text{ele}} \tag{7}$$

The electrolyzer's power output $\text{P}_{\text{ele}-\text{H}_2\text{t}}$, measured in kilowatts, is calculated by multiplying its input power $\text{P}_{\text{ren}_{\text{ele}}}$, also in kilowatts, by the constant efficiency factor η_{ele}.

2.4. Hydrogen tank modeling

During peak demand periods, when power generation from photovoltaic (PV) and wind sources is insufficient, a defined amount of stored hydrogen is supplied to fuel cells (FCs) to compensate for the energy

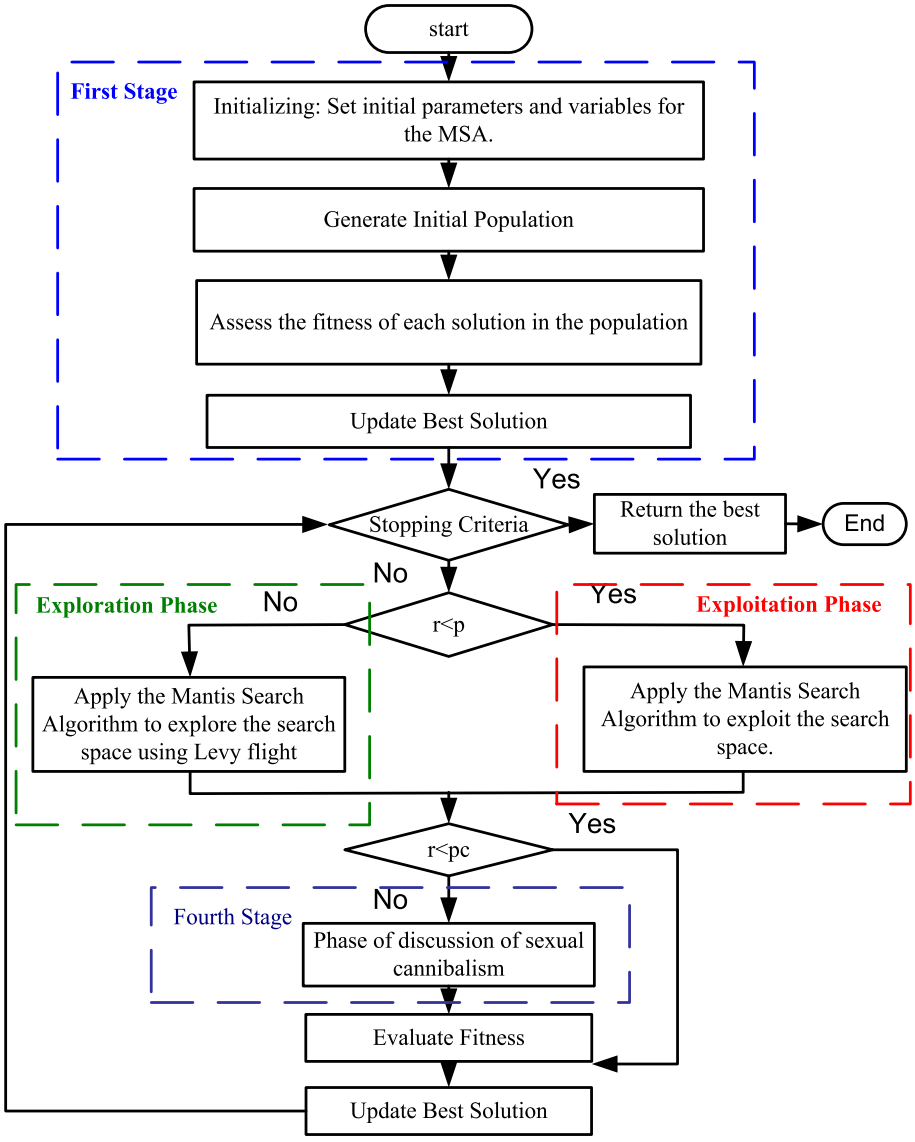

Fig. 2. Flowchart of the MSA optimization algorithm.

deficit. The hydrogen energy balance at any time step (t) is outlined as follows:

The quantities $E_{H_2t}(t)$ and $E_{H_2t}(t-1)$ represent the energy stored in the tank at times t and (t − 1), respectively. $P_{H_2t-fc}(t)$ denotes the power provided to the fuel cells. The efficiency of the hydrogen tank η_{st_t} is consistently assumed to be 95 % for all operations. The mass of hydrogen generated by the electrolyzers can be calculated using the following approach [52]:

$$M_{H_2t}(t) = \frac{E_{H_2t}(t)}{HHV_{H_2}} \tag{8}$$

The term HHV_{H_2} represents the higher heating value of hydrogen, standardized at 39.7 kWh/m^2.

The energy stored in the tank can be represented as follows:

$$E_{H_2t}(t) = E_{H_2t}(t-1) + \left(P_{ele-H_2t} - \frac{P_{H_2t-fc}(t)}{\eta_{st_t}}\right) \tag{9}$$

2.5. Fuel cell modeling

A fuel cell (FC) converts chemical energy into direct current (DC) electricity using an electrolyzer, where electrodes—anode and cathode—are separated by an electrolyte. Key advantages of fuel cells include operational simplicity, low maintenance requirements, high efficiency, and environmental compatibility. These characteristics establish fuel cells as a viable and sustainable energy source [53].

The power generated from the fuel cell can be calculated using Equation (10) as outlined below:

$$P_{fc-inv}(t) = P_{H_2t-fc}(t) \times \eta_{fc} \tag{10}$$

Here, P_{H_2t-fc} represents the power supplied to the fuel cell, and η_{fc} is the efficiency of the fuel cells.

3. Methodology

3.1. Strategy for operating hybrid systems

The operational procedures of the proposed hybrid renewable system are structured as follows:

i) When the combined electric energy generated by the PV and wind components surpasses the load demand, the surplus power is directed to the electrolyzer. The excess energy is employed to

convert water molecules into their constituents, oxygen (O_2) and hydrogen (H_2), storing the energy chemically in compressed H_2 tanks.

ii) If the surplus energy exceeds the electrolyzer's maximum consumption and the hydrogen tank is filled, the remaining difference is supplied to a dummy load. The dummy load power at time 't' is represented as:

$$P_{\text{dummy}}\ (t) = P_{\text{ren-inv}}\ (t) \times \eta_{\text{inv}}\ - P_{\text{load}}\ (t) \tag{11}$$

iii) In instances where the energy generated by the wind farm and PV system falls short of the load consumption, the deficiency is addressed by utilizing the stored hydrogen. This stored hydrogen is directed to the FC, where the chemical energy is converted into electrical energy to meet the load demand.

iv) When the quantity of stored hydrogen in the tank reaches its minimum permissible level, the shortfall is considered as LPS. The LPS at time 't' is determined by:

$$P_{Lps}(t) = P_{load}(t) - \left(P_{\text{ren-inv}}\ (t) + \mathrm{P}_{\text{fc-inv}}(t)\right) \times \eta_{inv} \tag{12}$$

The investigation into the optimal sizing of the hybrid energy system employs the MSA optimization algorithm, aiming to minimize the COE while ensuring the reliability of the proposed power supply system. The objective function involves achieving a reliability index (LPSP) below the predefined threshold of 5 %. The optimal sizing optimization problem and the details of the MSA algorithm are elaborated upon in the subsequent subsections.

3.2. Preparation of the optimization problem

The objective function is derived from the annual cost of units (kWh) produced by the developed hybrid system, encompassing various annual charges for each subsystem. These costs include the annual interest on capital investment ($(C_{\text{cap\_ann}})$), the annual replacement cost ($(C_{\text{rep\_ann}})$) for devices with a lifespan shorter than the entire system, the annual operation and maintenance cost ((C_{OM})), the annual penalty cost ((C_{pc})) applied when the reliability index and fluctuation level are unacceptable. The total annual cost of energy ($(C_{\text{tot\_ann}})$) is calculated as follows:

$$\left[C_{\text{tot\_ann}} = C_{\text{cap\_ann}} + C_{\text{rep\_ann}} + C_{OM} + C_{pc}\right] \tag{13}$$

As per references,[54,55], the net present cost (NPC) of the project (PV/wind/FC system) is expressed as:

$$\left[NPC = \frac{C_{\text{tot\_ann}}}{CRF}\right] \tag{14}$$

Here, CRF represents the capital recovery factor of the proposed energy system, calculated based on a 6 % rate of interest and a system lifespan of 25 years. The cost of energy (COE) in ($/kWh) to be minimized is formulated as:

$$\left[COE = \frac{NPC}{\sum_{i=1}^{8760} P_{\text{load}}(t_i)} \times CRF\right] \tag{15}$$

where (P_{load}) is the hourly load demand.

The minimization of COE is subject to specific operating conditions to ensure the effective and reliable performance of the power supply system. The defined minimum and maximum values for LPSP are zero and one, respectively. If LPSP = 0, the load demand will be completely met. Minimizing LPSP is a primary objective of this study, as the system exhibits greater reliability with reduced levels of LPSP. Therefore, the maximum quantity of LPSP was deemed to be 20 % [20]. The LPSP must be below the predefined reliability index value ($(\beta_L = 0.2)$).

These factors are computed and constrained as follows:

$$LPSP = \frac{\sum_{i=1}^{8760}\left(P_{\text{load}}(t_i) - \left(P_{PV}(t_i) + P_{WT}(t_i) + P_{FC-inv}(t_i)\right)\right)}{\sum_{i=1}^{8760} P_{\text{load}}(t_i)} \le \beta_L \tag{16}$$

$$P_{dump} = \frac{\sum_{i=1}^{8760} P_{\text{dummy}}(t_i)}{\sum_{i=1}^{8760} P_{\text{load}}(t_i)} \tag{17}$$

where P_{dump} denotes the ratio among the total dummy load to the total load demand.

A novel objective function, aiming to minimize the COE produced from the proposed system while adhering to the constraints, is expressed as:

$$min_x f = min_x\left(\sigma_1 \times COE + \sigma_2 \times LPSP + \sigma_3 \times P_{\text{dump}}\right) \tag{18}$$

Here, (x) is a vector representing the optimization parameters and $\sigma_1, \sigma_2,$ $and\, \sigma_3$ denote the weighting factors. The process of trial and error is used to accomplish the finest outcomes [56]. KLPSP ensures compliance with the LPSP constraint. It equals 1000 when LPSP exceeds a predefined threshold and 0 otherwise.

4. Developing mantis search algorithm (MSA) for optimizing the hybrid microgrid configuration

The mantis search algorithm (MSA) is influenced by the unique hunting behaviors and sexual cannibalism observed in praying mantises. MSA is composed of four optimization stages: Initializing, exploring for prey, attacking prey, and incorporating sexual cannibalism. These stages are simulated using diverse mathematical models, effectively addressing optimization challenges across varied search spaces. The first stage involves the mathematical representation of mantis locations, symbolizing the initialization of the population. The second stage encompasses the exploration phase, the third stage focuses on the exploitation phase, and the fourth stage involves the discussion of sexual cannibalism. Before commencing the optimization procedure, specific parameters are defined for MSA. Parameters include T for the maximum number of iterations, A for the length of an archive, N for the population size, p for the probability of exchange between the exploitation and exploration stages, for the probability of strike failure, ρ for the gravitational acceleration rate of the mantis's strike, P for the recycling factor that balances between spearers and pursuers, and Pc for estimating the percentage of sexual cannibalism. Fig. 2 provides the flowchart outlining the MSA process. The details mathematical representation of the MSA can be found in [57].

Within the MSA, the search mechanisms are meticulously crafted to harmonize exploration and exploitation, ensuring an efficient traversal of the solution space. MSA strives to strike a balance between these two facets by amalgamating distinct search mechanisms. The synergy of random search and global search mechanisms fosters exploration, diversifying the population and venturing into novel regions. Simultaneously, the local search mechanism exploits and refines promising solutions.

The adaptive search mechanism plays a pivotal role in dynamically adjusting the equilibrium between exploration and exploitation, guided by the algorithm's performance. This dynamic adjustment ensures an adept and efficient search process that effectively navigates and exploits the solution space. In the flowchart, the diamond signifies the adaptive control governing the interplay between exploration and exploitation characteristics. Here, a probability (p) of 50 % is employed to facilitate the exchange between the exploration and exploitation stages. The mathematical representation of the MSA algorithm can be formulated as:

4.1. Initial population

The algorithm begins by initializing the population of mantises. Each

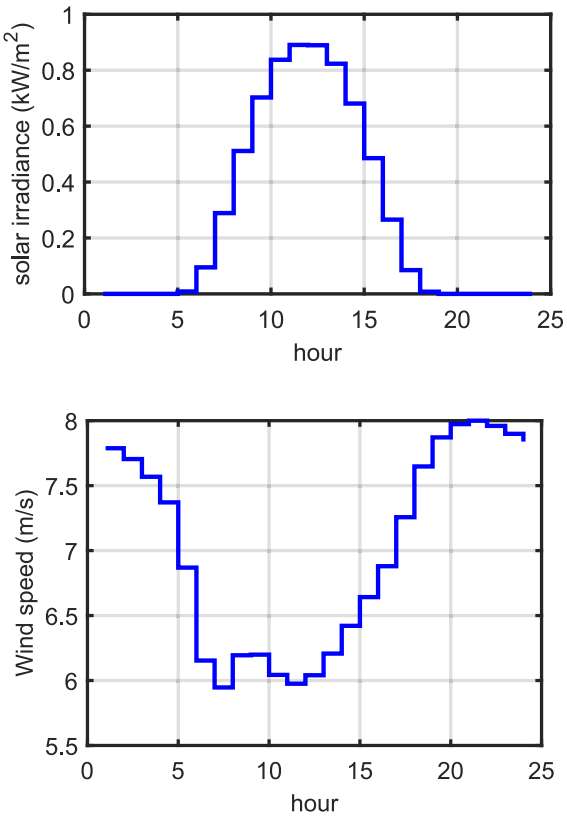

Fig. 3. Discrepancy of site data; average hourly over the year; (a) solar radiation, (b) wind speed.

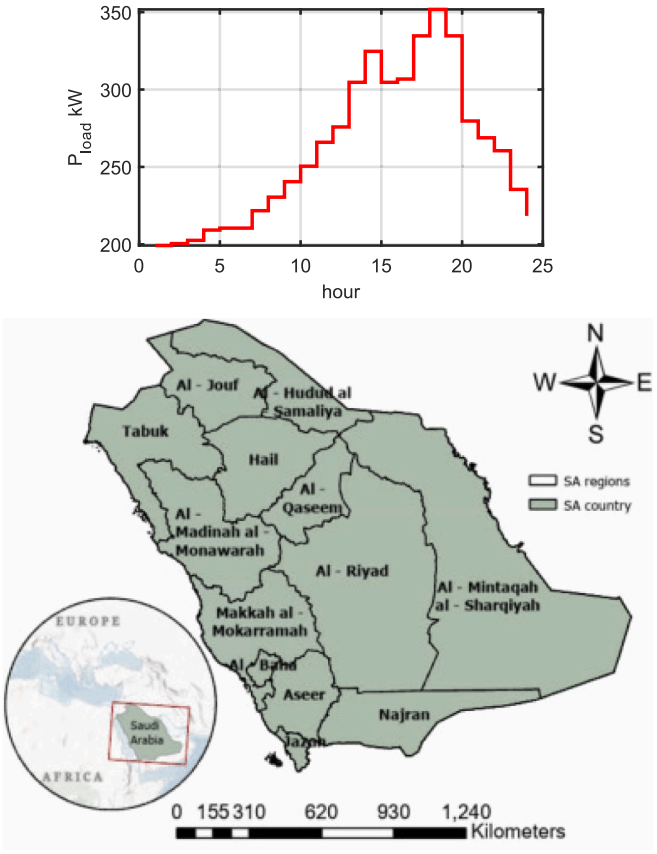

Fig. 4. A) average hourly load demand over the year at the selected site and b) Fig. 6. Location of the case study (Najran, in southern KSA).

mantis represents a candidate solution to an optimization problem. The initial population of N mantises in a D-dimensional search space is represented by a matrix x of size $N \times D$.

The position of the i^{th}h mantis at iteration t is defined as a vector initialized randomly within the problem's bounds:

$$x_i^t = x_l + r \cdot (x_u - x_l), \tag{19}$$

where, x_u and x_l represent the upper and lower bounds of the j^{th} dimension. Moreover, r denotes a random vector with values uniformly distributed between 0 and 1.

Each mantis's effectiveness is assessed using a fitness function. If a new location yields a better solution, the mantis moves there; otherwise, it stays in place.

4.2. Search for prey: Exploration stage

Mantises exhibit two types of behaviors during the exploration of Pursuers which is the Actively searching for prey by moving through different regions and Spearers which is Stay camouflaged and ambush prey.

4.2.1. Pursuers' behavior

The pursuers' exploration is modeled using a hybrid strategy that combines Lévy flight and normal distribution to balance step sizes. The mathematical model for pursuers' movement is given by:

$$x_i^{t+1} = \begin{cases} x_i^t + \tau_1 \cdot (x_i^t - x_a^t) + \tau_2 \cdot U \cdot (x_a^t - x_b^t), \text{if } r_1 \le r_2, \\ x_i^t \cdot U + x_a^t + r_3 \cdot (x_b^t - x_c^t) \cdot (1 - U), \text{otherwise}, \end{cases} \tag{20}$$

where, x_i^t denotes the position of the i-th mantis at iteration t. τ_1 denotes the vector generated using Lévy flight. τ_2 denotes a random number from a normal distribution with mean 0 and standard deviation 1.

Table 2
The technical specifications of different components within the planned system.

Component	Capital Cost (US $/unit)	Repl. cost (US $/unit)	M cost (US $/unit-yr)	Lifetime (yr)	Effic. (%)	Unit
Wind [58]	11,000	10,000	30	20	–	10 kW
PV [58]	400	400	10	25	–	1 kW
Electrolyzer [59]	1500	1500	25	20	75	1 kW
Hyd. Tank [59]	700	700	15	20	95	1 kg
Fuel cell [59]	2000	2000	175	5	50	1 kW
DC/AC Conv. [58]	200	200	1	15	90	1 kW

Moreover, r_1, r_2, r_3 are random numbers uniformly distributed between 0 and 1, while x_a^t, x_b^t, x_c^t are randomly selected solutions from the population ($x_a^t \neq x_b^t \neq x_c^t \neq x_i^t$). U represents binary vector which can be determined as:

$$U_j = \begin{cases} 0, r\_4 < r\_5 \\ 1, otherwise \end{cases} \tag{21}$$

where r_4, r_5 are random numbers uniformly distributed between 0 and 1.

4.2.2. Spearers' behavior

Spearers remain stationary and ambush prey. This behavior is modeled by constructing an archive of the best solutions and updating their positions based on prey movement. The mathematical model is:

TABLE 3
Results of the system designed based on MSA algorithm.

Configuration	Configuration 1 PV/wind/FC	PV/wind/FC	PV/wind/FC	PV/wind/FC	Configuration 2 PV /FC	PV /FC	PV /FC	PV /FC
Case	Case 1-Config 1	Case 2-Config 1	Case 3-Config 1	Case 4-Config 1	Case 1-Config 2	Case 2-Config 2	Case 3-Config 2	Case 4-Config 2
obj_cost	0.1*COE+ 0.1*P_dum+ 0.8*LPSP	0.2*COE+ 0.2*P_dum+ 0.6*LPSP	0.2*COE+ 0.2*P_dum+ 0.6*LPSP+ KLPSP	0.1*COE+ 0.1*P_dum+ 0.8*LPSP+ KLPSP;	0.1*COE+ 0.1*P_dum+ 0.8*LPSP	0.2*COE+ 0.2*P_dum+ 0.6*LPSP	0.1*COE+ 0.1*P_dum+ 0.8*LPSP+ KLPSP	0.2*COE+ 0.2*P_dum+ 0.6*LPSP+ KLPSP
Best objective function	0.066583	0.096356	0.098046	0.066583	0.156387	0.244733	0.156386	0.266870
PV (units)	557.3844	383.1594s	406.3768	557.4693	3464.684	2602.796	3464.663	3257.109
Wind (units)	119.0065	96.71602	101.9845	119.0213	–	–	–	–
Electrolyzer (kW)	734.6092	491.0164	550.3073	736.3357	2221.152	1618.843	2221.705	2033.427
Hydrogen tank (kg)	257.9347	156.071	172.6082	257.9353	515.8707	271.5453	515.8693	372.422
Fuel cell (kW)	130.5979	69.40371	75.91922	131.262	373.6823	314.0313	373.6835	362.9108
iterations	18	16	18	18	20	19	19	19
Cost ann. tot. (US$)	5.4106E + 05	3.6717E + 05	3.9856E + 05	5.4218E + 05	1.1399E + 06	8.6691E + 05	1.1400E + 06	1.0587E + 06
COE(US$/kWh)	0.237477	0.161154	0.174933	0.23797	0.500295	0.380493	0.500352	0.4646543
LPSP (%)	0.022570	0.057322	0.04978	0.022517	0.036985	0.099117	0.036986	0.049997
Dummy load	0.2477888	0.1486598	0.165956	0.247718	0.767687	0.545822	0.76762438	0.7197066
Time (sec.) (average 208.4752 sec)	211.3860	197.5983	250.2866	207.2957	147.0929	197.7074	216.7183	239.7164

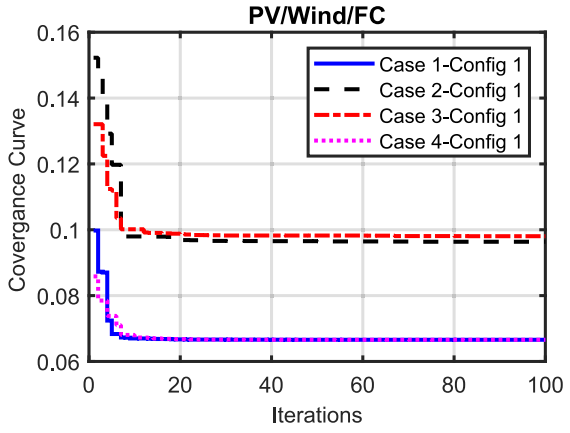

a)

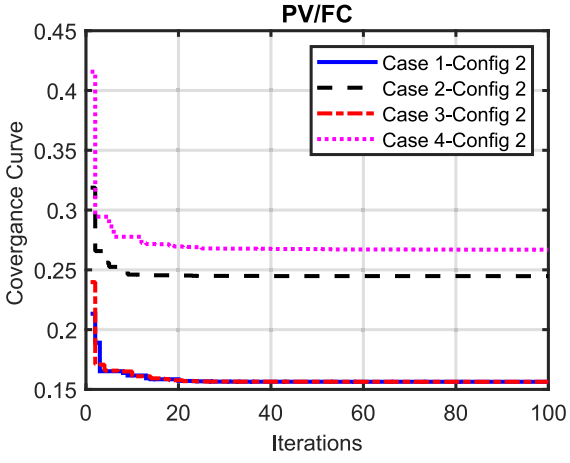

b)

Fig. 5. Convergence curves of the MSA for the two studied systems, a) PV/wind/FC and b) PV /FC.

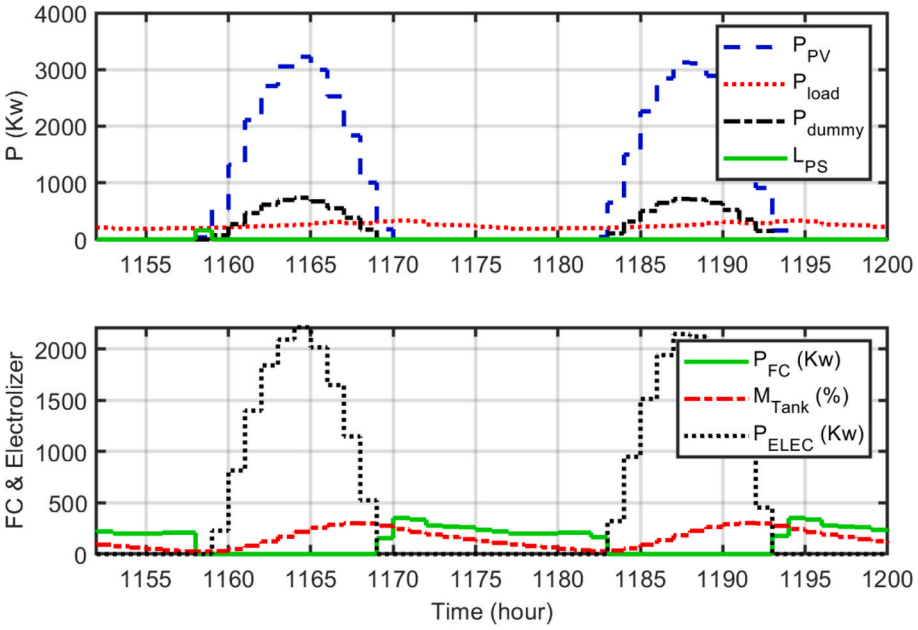

Fig. 6. Operation of the proposed PV /FC off-grid hybrid energy system.

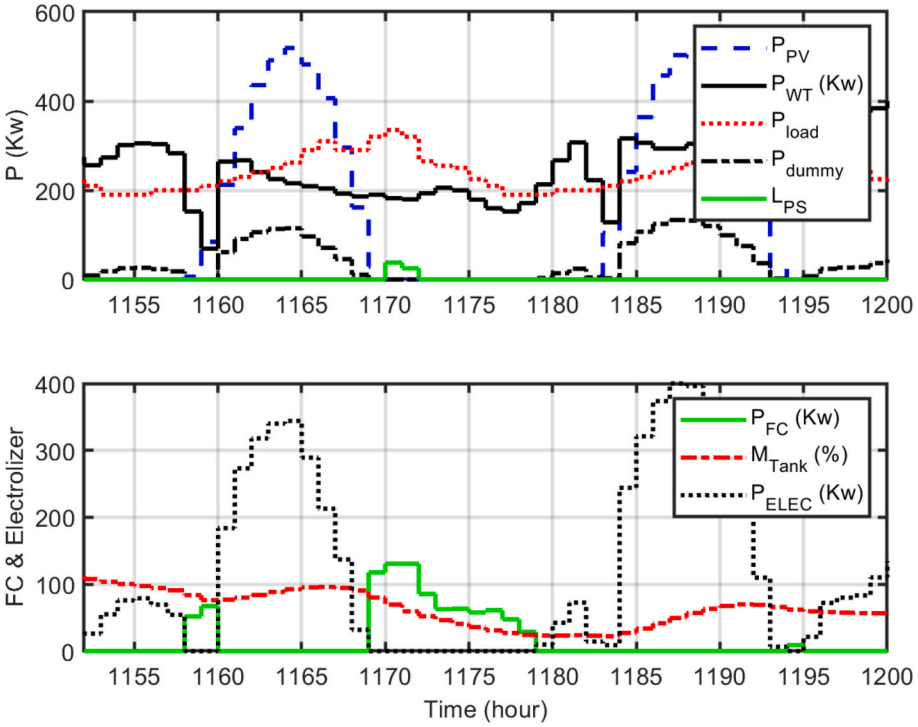

Fig. 7. Operation of the proposed PV/wind/FC off grid hybrid energy system.

$$x_i^{t+1} = x_i^t + \alpha \cdot (x'_{ar} - x_a^t), \tag{22}$$

where, x'_{ar} is a random solution from the archive. α is a factor controlling the ambush distance, that can be defined as:

$$\alpha = \cos(\pi r_6) \cdot \mu, \tag{23}$$

With considering r_6 as a random number uniformly distributed between 0 and 1. And μ is the distance factor, which can be computed as:

$$\mu = 1 - \frac{t}{T}, \tag{24}$$

where T is the maximum number of iterations.

4.3. Combined exploration

The prey's movement within the ambush region is modeled as:

$$\vec{x}_i^{t+1} = \begin{cases} \vec{x}_i^t + \alpha \cdot \left(\vec{x}'_{ar} - \vec{x}_a^t \right), & r_9 \le r_{10} \\ \vec{x}'_{ar} + (r_7 * 2 - 1) * \mu * \left(\vec{x}^l + \vec{r_8} \times \left(\vec{x}^u - \vec{x}^l \right) \right), & Otherwise \end{cases}, \tag{25}$$

TABLE 4
Statistical indices for the two proposed configurations hybrid systems.

	PV/wind/FC	PV/FC
Metric	Case 1-Config 1	Case 1-Config 2
Mean	0.0666	0.1564
Median	0.0666	0.1564
Min	0.0666	0.1564
worst	0.0666	0.1564
SD	5.5039e-06	5.6091e-06
RE	1.1993e-05	4.4793e-06
MAE	7.9850e-08	7.0050e-08
RMSE	9.5407e-08	8.7969e-08
Efficiency	99.9999	100.0000
Wilcoxon signed rank		
p	0.0020	0.0020
h	1 (logical)	1 (logical)

where r_7, r_8, r_9, r_{10} are random numbers uniformly distributed between 0 and 1.The exploration phase is balanced using a recycling control factor F:

$$F = 1 - \frac{t\%\left(\frac{T}{P}\right)}{\frac{T}{P}}, \tag{26}$$

where P is the number of cycles.

4.3.1. Attacking the Prey: Exploitation stage

Mantises use stealth and precision in predation, relying on visual triangulation to estimate strike distance and velocity for effective captures. Their strike distance typically ranges from 70 %–80 % of their foreleg length, with optimal strikes occurring at 30 %–40 %. Binocular triangulation through their triangular head and compound eyes enables accurate distance measurement. Strikes are ballistic, predetermined by visual and proprioceptive data, with corrective pauses addressing initial speed estimation errors. These behaviors inspire mathematical models in the mantis search algorithm, simulating natural strategies for optimization.

4.3.2. Strike velocity

Strike velocity can be modeled using a sigmoid function:

$$v_s = \frac{1}{1 + e^{l\rho}} \tag{27}$$

where, v_s is strike velocity. ρ represents a constant gravitational acceleration rate. l is a random value $-1 \le l \le -2$).

4.3.3. Position update

The mantis updates its position by combining prey location, strike distance, and velocity:

$$x_{i,j}^{t+1} = x_{i,j}^{t} + \frac{x_j^*}{2.0} + v_s \cdot \left(x_j^* - x_{i,j}^{t}\right) \tag{28}$$

$x_{i,j}^{t+1}$ is the updated position. x_j^* represents the prey position. $x_{i,j}^{t}$ denotes current position.

4.3.4. Failed strikes

When a strike fails, the mantis adjusts direction:

$$x_{i,j}^{t+1} = x_{i,j}^{t} + r_{12} \cdot \left(x_{a,j}^{t} - x_{b,j}^{t}\right) \tag{29}$$

where, $x_{a,j}^{t}, x_{b,j}^{t}$ represents the random mantis positions. r_{12} is the random factor ($0 \le r_{12} \le 1$).

Additional adjustments enhance diversity and avoid stagnation:

$$x_{i,j}^{t+1} = x_{i,j}^{t} + e^{2l} \cdot \cos(2l\pi) \cdot \left(x_{i,j}^{t} - x_{ar,j}^{t}\right) + r_{13} \cdot \left(x_{j,u} - x_{j,l}\right) \tag{30}$$

where, $x_{ar,j}^{t}$ is the random mantis position. $x_{j,u}, x_{j,l}$ are the upper and

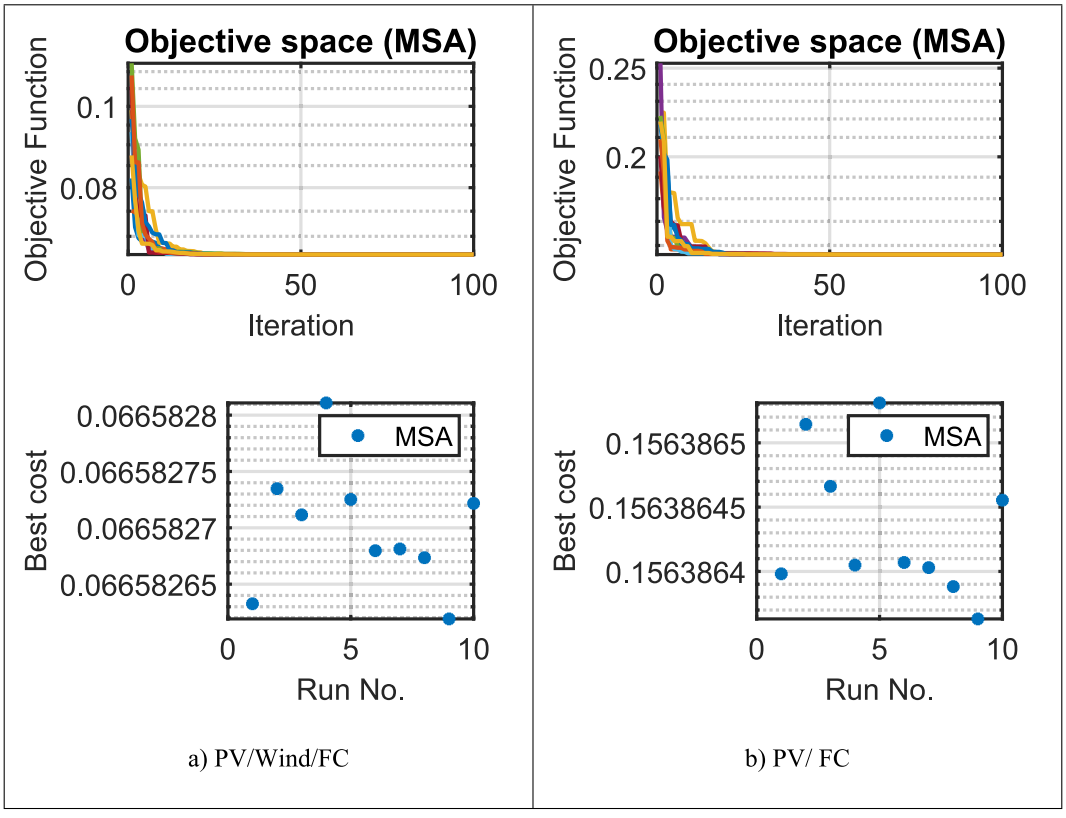

Fig. 8. The results of 10 individual runs using MSA: a) PV/Wind/FC and b) PV/ FC.

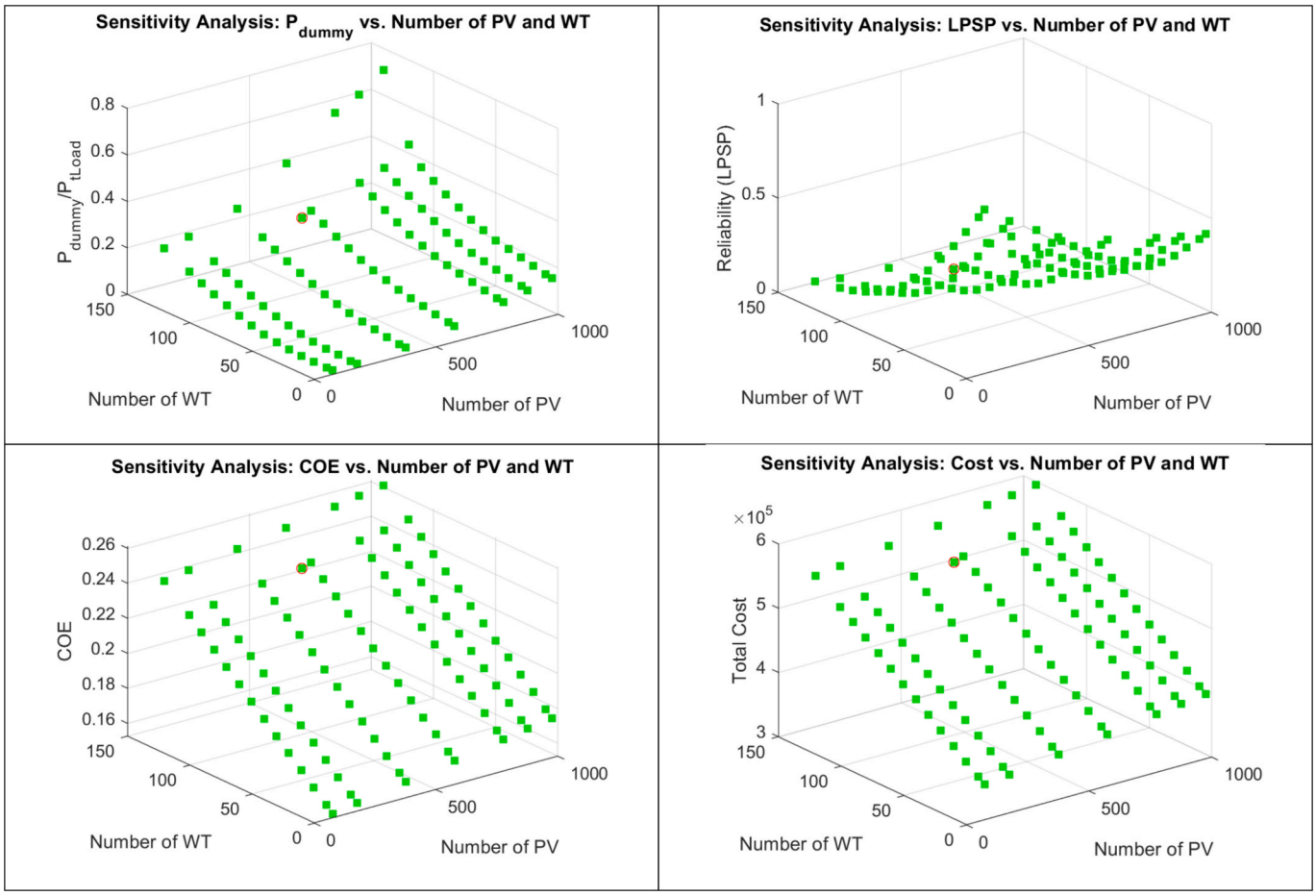

Fig. 9. Sensitivity analysis considering the variation in the PV and WT at fixed values of other components for PV/Wind/FC.

lower bounds. r_{13} represents the random value ($0 \le r_{13} \le 1$).

4.4. Exploration vs. Exploitation probability

$$P_f = a \cdot \left(1 - \frac{t}{T}\right) \tag{31}$$

where, a represents the control parameter. t is the current iteration. T denotes the total iterations.

4.5. Sexual cannibalism mechanism

4.5.1. Mate attraction

Female mantises attract males using position updates:

$$x_i^{t+1} = x_i^t + r_{16} \cdot \left(x_i^t - x_a^t\right) \tag{32}$$

where, r_{16} is a random attraction factor.

4.5.2. Mating

Offspring positions are generated using uniform crossover:

$$x_i^{t+1} = x_i^t \cdot U + x_{11}^t + r_{18} \cdot \left(x_{11}^t - x_i^t\right) \cdot (1 - U) \tag{33}$$

where, U is the uniform crossover factor.

4.5.3. Cannibalism

After mating, females consume males to enhance diversity:

$$x_i^{t+1} = x_a^t \cdot \cos(2\pi l) \cdot \tag{34}$$

where, μ is the fraction of male consumed.

This stage integrates biological hunting and mating behaviors into optimization models. Strike distance, velocity, and failed strike adjustments ensure effective exploitation. Sexual cannibalism diversifies solutions while maintaining exploration–exploitation balance.

5. Results and discussion

5.1. Case study

This paper explores the optimal sizing of a proposed hybrid energy system using the MSA optimization technique. The study considers two scenarios: the first scenario involves a hybrid system consisting of PV, WT, and FC, whereas the second scenario comprises a hybrid system with PV and FC. By analyzing these scenarios, this study aims to determine the most efficient and effective configuration for an energy system. A practical case study was conducted in Najran, KSA (latitude 17.4924 °N and longitude 44.1277 °E). The geographical location of Najran, characterized by a high intensity of solar radiation and consistent wind flow, makes it exceptionally suitable for renewable energy initiatives. Fig. 3 illustrates the average hourly intensity of solar radiation, and the average hourly wind speed observed at the chosen site. Moreover, the fixed-tilt alternatives for monthly, seasonal, and annual assessments have all been analyzed, and the optimal one has been selected. The annual optimal tilt for Najran was determined to be 20.97°, as indicated in [4]. Additionally, the average hourly load demand of 260.0888 kW at this location is depicted in the load graph in Fig. 4.a. Fig. 4.b shows the location of the study area in southern KSA. Table 2 summarizes the technical specifications of the different components of the planned system. The annual interest rate is selected to be

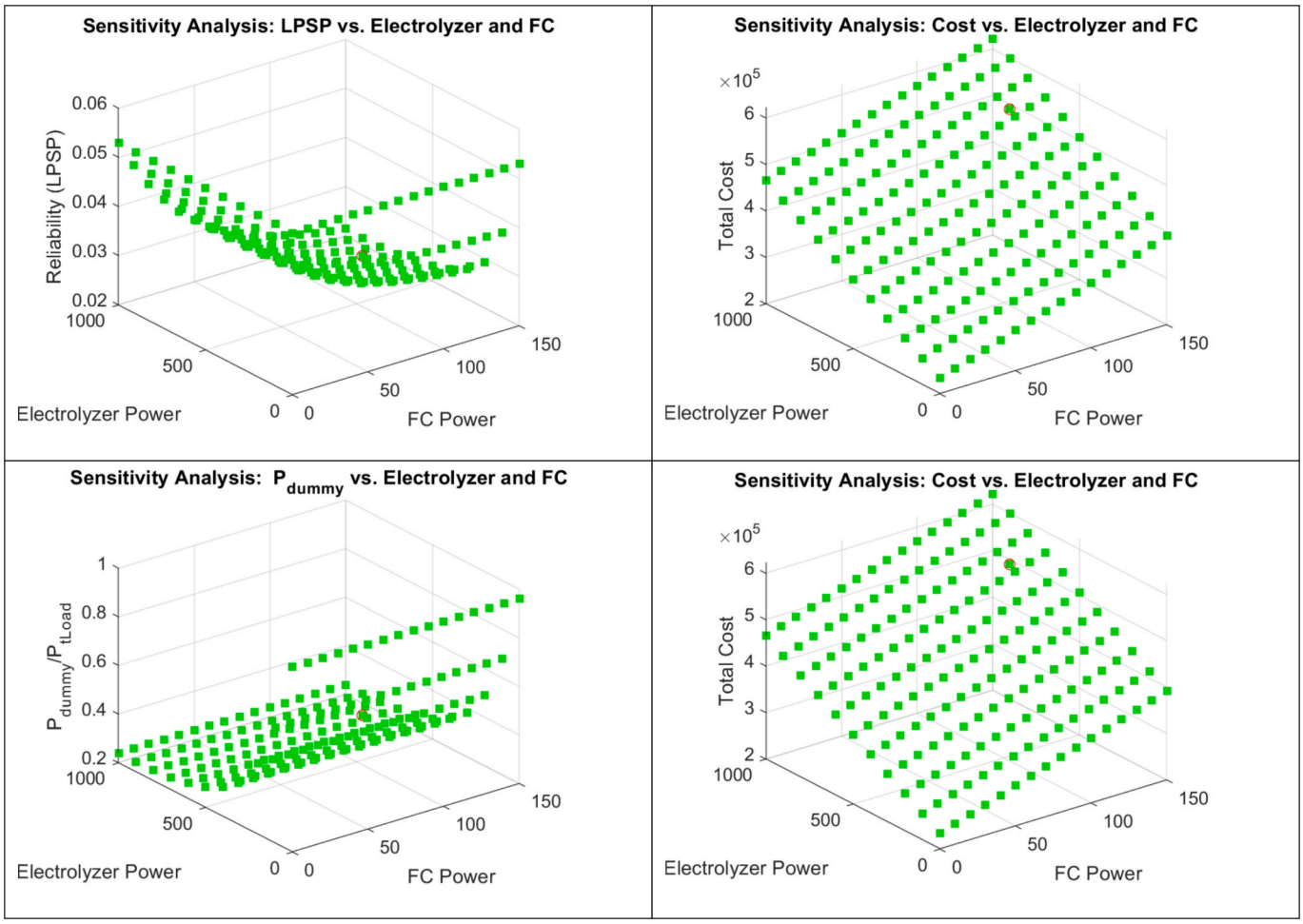

Fig. 10. Sensitivity analysis considering the variation in the Electrolizer and FC power at fixed values of other components for PV/Wind/FC configuration.

6 % and the project lifetime is 25 years.

5.2. Optimal configuration

The validation of the optimization program extends to the entire system, encompassing the PV, wind, and FC subsystems. To further scrutinize the reliability and precision of the proposed MSA technique, the optimization program was evaluated in distinct scenarios involving PV and wind power plants. Across all instances, the optimization program underwent 10 individual runs, and a statistical analysis of the objective function values is conducted. Throughout the simulation, the maximum iteration count is set to 50 and the maximum population size is 20. The boundaries and search space for the variables have been set between 1 and 4000 for each variable in vector x. The MSA implementation has been carried out using MATLAB version R2023b on a Laptop with an Intel Core i7-10510U CPU @ 1.80 GHz, 2.30 GHz processor, 16 GB of RAM, and running the Windows 11 Pro (64-bit) platform.

The Mantis Shrimp Algorithm (MSA) was applied to solve the photovoltaic (PV) model extraction problem using specific parameter settings. The probability of switching between exploration and exploitation stages was set to $p = 0.5$, allowing a balanced search process. The archive length (A) was set to 1.0 to maintain a single elite solution. The probability of a strike failure was defined as $a = 0.5$, introducing variability in local exploitation. A recycling factor $P = 2$ controlled the dynamic exchange between pursuers and spearers during the search process. The gravitational acceleration of the mantis's strike, represented by $\alpha = 6$, influenced the convergence speed of the algorithm. Moreover, the percentage of sexual cannibalism was set to $P_c = 0.2$, which helped increase solution diversity and reduce the risk of premature convergence.

For validating the microgrid configurations, there are 4 objective functions have been tested for each system. The four objective functions are based on equation (18). The values of the $\sigma_1, \sigma_2,$ *and* σ_3 have been varied from one case to another. Moreover, the KLPSP factor has been considered in two studied cases for each system configuration. The values of the $\sigma_1, \sigma_2,$ *and* σ_3 have been listed for the four objective functions in Table 3. The average time during the run of the MSA for the 8 cases of study is 208.4752 Sec.

Table 3 presents the performance comparison of two system configurations—PV + Wind + FC (Configuration 1) and PV + FC (Configuration 2)—each evaluated across four cases with distinct objective functions. The results highlight the impact of different optimization priorities on system cost, reliability, and energy efficiency.

Among all cases, Case 1 of Configuration 1 (PV + Wind + FC) achieves the best overall performance, with an objective function value of 0.066583, a low LPSP of 0.02257 %, and moderate COE (0.2375 USD/kWh). This case effectively balances cost and reliability, ensuring minimal unmet energy demand while maintaining an affordable cost of energy. Moreover, its dump load (0.2478) is relatively low, indicating efficient energy utilization.

For Configuration 2 (PV + FC), Case 1 also emerges as the best-performing scenario, with an objective function value of 0.156387, LPSP of 0.036985 %, and COE of 0.5003 USD/kWh. However, its dump load (0.7677) is significantly higher than that of Configuration 1, suggesting greater energy wastage. Additionally, despite having the lowest

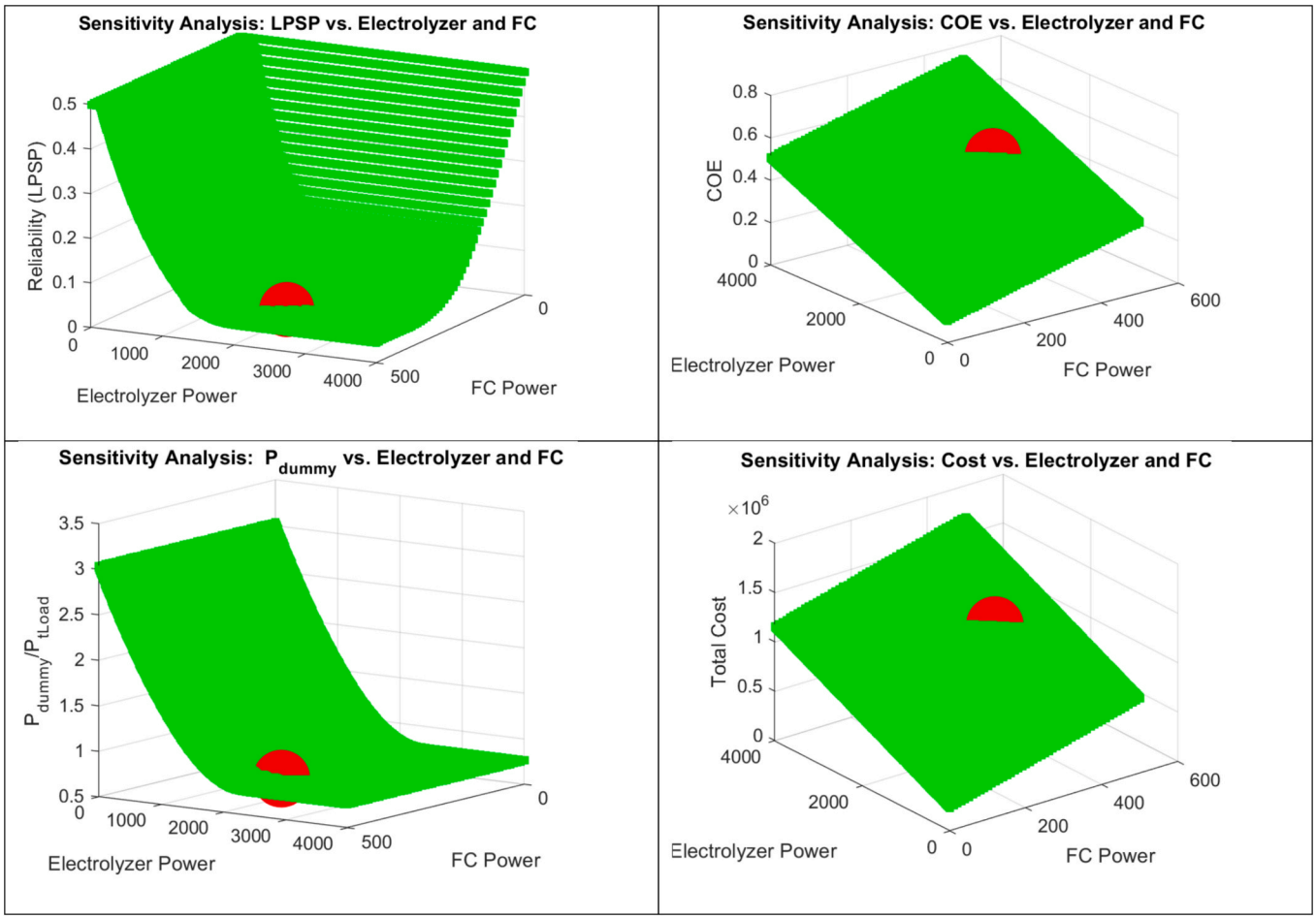

Fig. 11. Sensitivity analysis considering the variation in the Electrolizer and FC power at fixed values of other components for PV/FC configuration.

LPSP among the cases in Configuration 2, its COE is more than double that of Configuration 1, making it a less cost-effective option.

In Configuration 1 (PV + Wind + FC), the four cases reflect different trade-offs between system cost, LPSP, and energy efficiency. Case 4 achieves an equally low LPSP (0.022517 %) compared to Case 1, but the inclusion of KLPSP in the objective function leads to a slightly higher cost (0.23797 USD/kWh), making it less favorable. Case 2 and Case 3, which prioritize COE and dump load, exhibit higher LPSP values (0.057322 % and 0.04978 %) and slightly lower COE (0.1612 and 0.1749 USD/kWh, respectively). While these cases reduce cost, they compromise reliability, making them less suitable for applications where uninterrupted power supply is crucial.

In Configuration 2 (PV + FC), LPSP values are consistently higher than in Configuration 1, confirming that the absence of wind power reduces system reliability. Case 4 exhibits the highest objective function value (0.266870) due to KLPSP enforcement, indicating a significant cost increase to meet LPSP constraints. Cases 2 and 3 show a moderate reduction in COE (0.3805 and 0.5004 USD/kWh, respectively) but suffer from high LPSP values (0.099117 % and 0.036986 %). Overall, Configuration 2 struggles to achieve both low COE and low LPSP simultaneously, making it a less efficient and cost-effective choice.

The results confirm that Case 1 of Configuration 1 (PV + Wind + FC) is the best overall scenario, providing low LPSP (0.02257 %), reasonable COE (0.2375 USD/kWh), and minimal energy waste. The integration of wind power significantly enhances system performance by reducing LPSP while maintaining cost-effectiveness. In contrast, Configuration 2 (PV + FC) exhibits higher COE and dump load across all cases, making it a less viable option despite some improvements in specific scenarios. These findings highlight the importance of selecting an appropriate energy mix to balance cost, reliability, and efficiency.

The inclusion of the wind turbine in the hybrid system helps manage energy more effectively, reducing the need for dump loads and improving overall system efficiency. Although the dump load ratio is huge in the two systems, especially in the PV + FC system, one should note that the two systems did not meet the constraint of the LPSP value of 5 %. A demand-side management could improve the system's performance. One should note that in order to maintain the LPSP value within its limits, the cost of the system may be increased. Such case study has been analyzed and the results have been shown in Table 3.

The convergence curves of the objective functions for the two systems are depicted in Fig. 5. The convergence curves show that the MSA has a fast convergence speed among 18 and 29 iterations for the 8 cases of study, to converge the best value of the objective function. One reason for the lower COE is the use of the wind turbine (WT), which helps meet load demand during the night when there is no sunlight, thereby reducing reliance on energy storage. So, the addition of the wind turbine in the hybrid system reduces dependency on fuel cells and energy storage, leading to a more cost-efficient solution.

The overall system operation is visualized by utilizing the optimal results from the PV/wind/FC and PV /FC off-grid hybrid energy systems, as presented in Table 3 for Case 1-Config 1 and Case 1-Config 2. The performance during a specific time (48-hour simulation) is illustrated in Figs. 6 and 7. The figures show the load demand, renewable generation, and resultant variance between them (dummy and LPS power). Meanwhile, the figures elucidate the operation of the electrolyzer, fuel cell (FC), and tank. Fig. 6 shows the operation of the proposed PV/FC off-grid hybrid energy system. While Fig. 7 shows the operation of the proposed PV/Wind/FC hybrid energy system. It should be noted that the

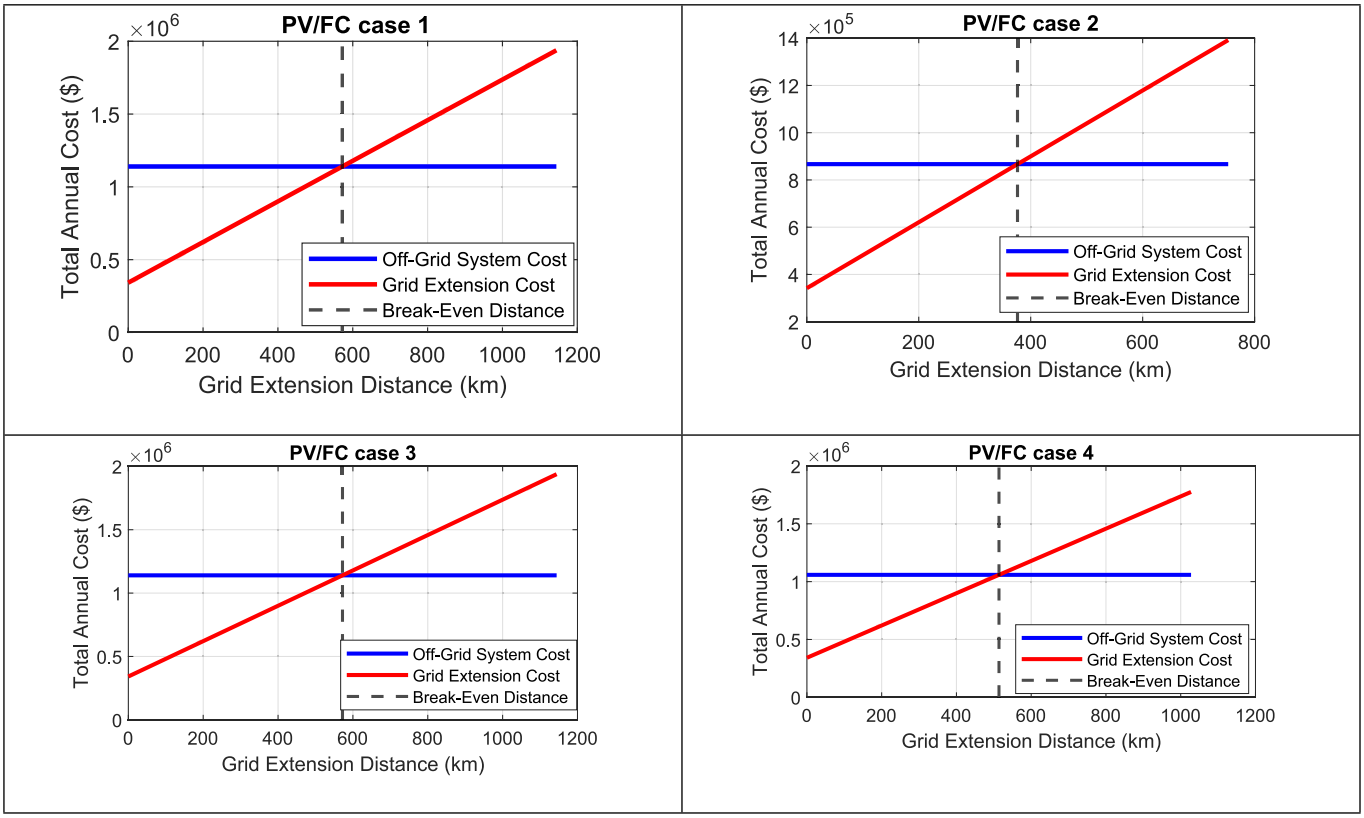

Fig. 12. Break-Even Grid Extension Distance Analysis for the cases of PV/FC configuration.

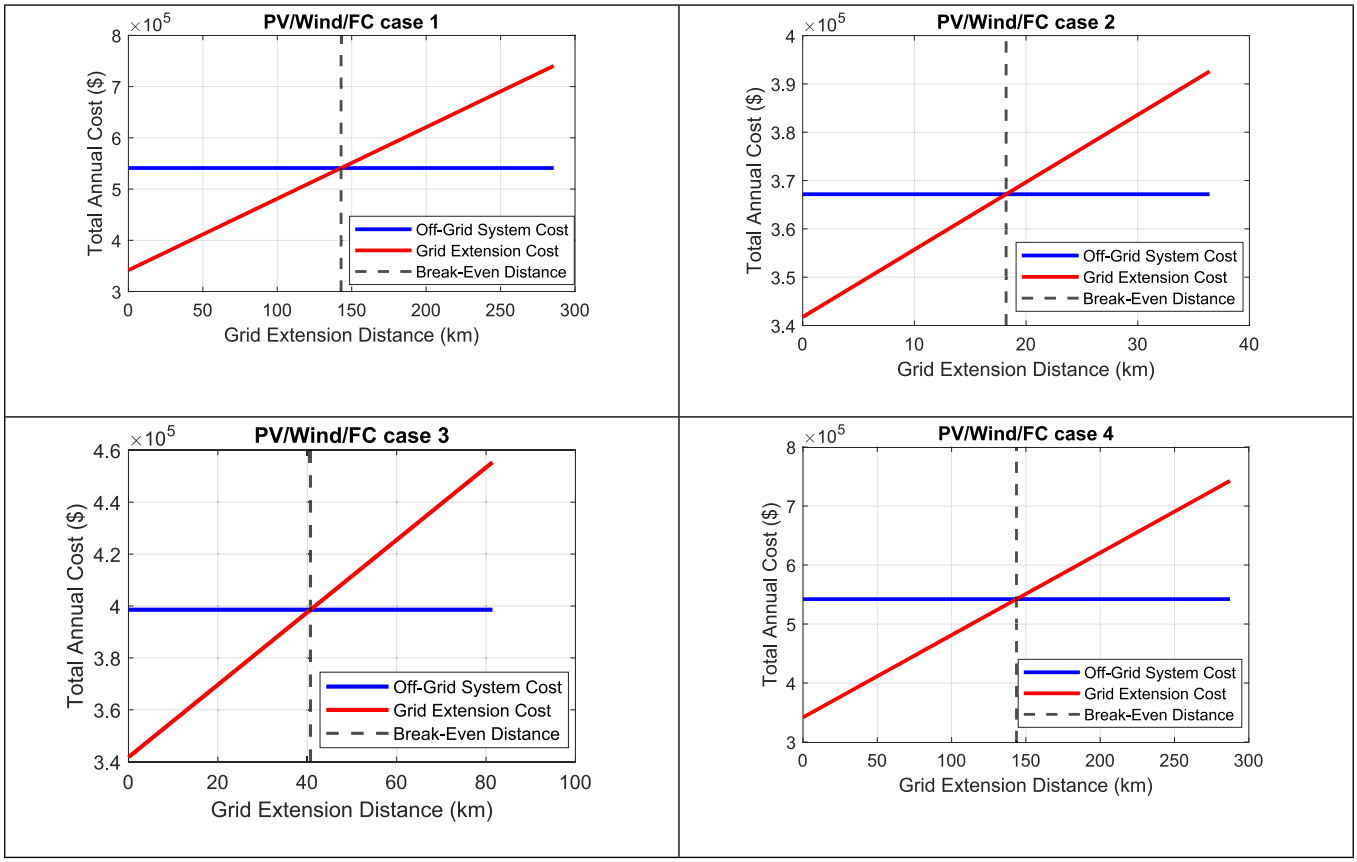

Fig. 13. Break-Even Grid Extension Distance Analysis for the cases of PV/Wind/FC configuration.

Table 5
Comparative performance metrics for PV/Wind/FC and PV/FC hybrid energy systems optimized using WOA, DOMA, and the proposed MSA.

	PV/Wind/FC using WOA	PV/Wind/FC using DOMA	PV/Wind/FC using MSA	PV /FC using WOA	PV/ FC using DOMA	PV/ FC using MSA
	PV/Wind/FC			PV /FC		
COE	0.223004	0.240968	0.237477	0.442573	0.515905	0.500295
LPSP	0.025811	0.022149	0.022570	0.065506	0.028874	0.036985
P_dum	0.244696	0.248852	0.2477888	0.625022	0.82122	0.767687
n_PV	447.1246	517.3104	557.3844	2893.362	3660.374	3464.684
n_WT	127.2209	124.107	119.0065	0	0	–
P_ELEC_rated	701.2022	778.0097	734.6092	1784.264	2331.823	2221.152
M_Tank_max	268.1961	258.5637	257.9347	319.9784	520.8169	515.8707
P_FC_rated	99.18108	123.2906	130.5979	393.0788	373.1475	373.6823
TIME (SEC.) (for the 10 individual runs)	Average ≈ 41.5492 Minimum = 34.7607 Maximum = 48.0188	Average ≈ 66.0793 Minimum = 55.4594 Maximum = 91.4013	Average≈ 236.24 Minimum≈ 174.67 Maximum≈ 286.84	Average ≈ 40.2862 Minimum = 32.8673 Maximum = 47.5558	Average ≈ 72.4486 Minimum = 63.4912 Maximum = 101.6409	Average≈ 236.05 Minimum≈ 177.85 Maximum≈ 294.76

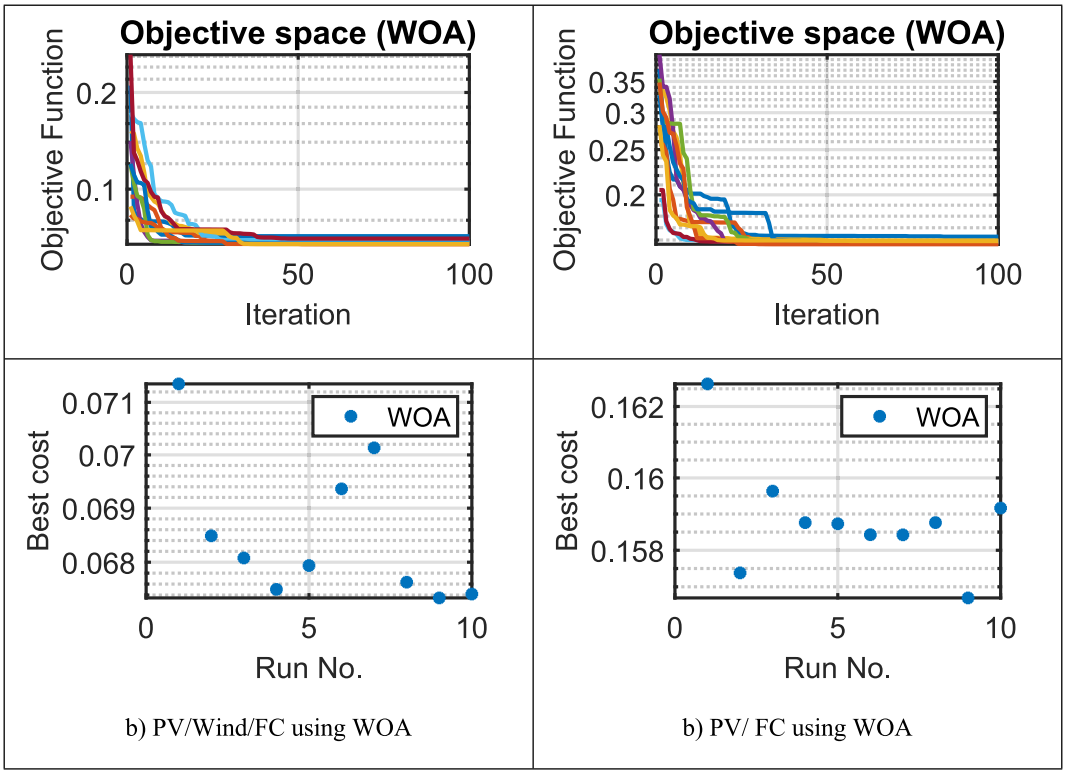

Fig. 14. The results of 10 individual runs using using WOA: a) PV/Wind/FC using WOA and b) PV/ FC using WOA.

dummy load and LPS in the PV/FC system were higher than those in the PV/Wind/FC system. It is recommended to use the excess energy in industrial applications and for hydrogen production.

5.3. Statistical analysis

The reliability of the MSA algorithm for optimizing the considered nonlinear optimization problem of sizing the RES has been ensured through statistical analysis and validation by conducting multiple individual runs. The statistical results have been conducted for the for Case 1-Config 1 and Case 1-Config 2. The results of the statistical analysis are presented in Table 4. The negligible values observed in various metrics, including the relative error (RE), root mean square error (RMSE), and standard deviation (SD), provide compelling evidence to confirm the stability of the proposed system. Although MSA generates diverse values of the objective function in each run, the presence of a smaller overshoot attests to the robustness of the system. Moreover, the results of 10 individual runs have been shown in Fig. 8. The results show the reliability and effectiveness of the MSA considering the lower value of SD of 5.5039e-06 and 5.6091e-06 for PV/Wind/FC and PV/FC configurations, respectively. The Efficiencies of the MSA algorithm to get the optimal value over the individual runs are 99.9999 % and 100 % for PV/Wind/FC and PV/FC configurations, respectively. Mean Absolute Error (MAE) and Root Mean Square Error (RMSE) are calculated for both configurations. The MAE for PV/Wind/FC is 7.9850e-08 and for PV/FC is 7.0050e-08. moreover, the RMSE for PV/Wind/FC: 9.5407e-08 and PV/FC is 8.7969e-08. the results are minimal in both cases, showing high precision in terms of reliability. The PV/Wind/FC configuration records a consistent cost value of 0.0666 across the mean, median, minimum, and worst-case metrics, while the PV/FC setup shows a higher value of 0.1564 for all four. This uniformity in the PV/Wind/FC results suggests a more stable and controlled system response. The consistently lower cost

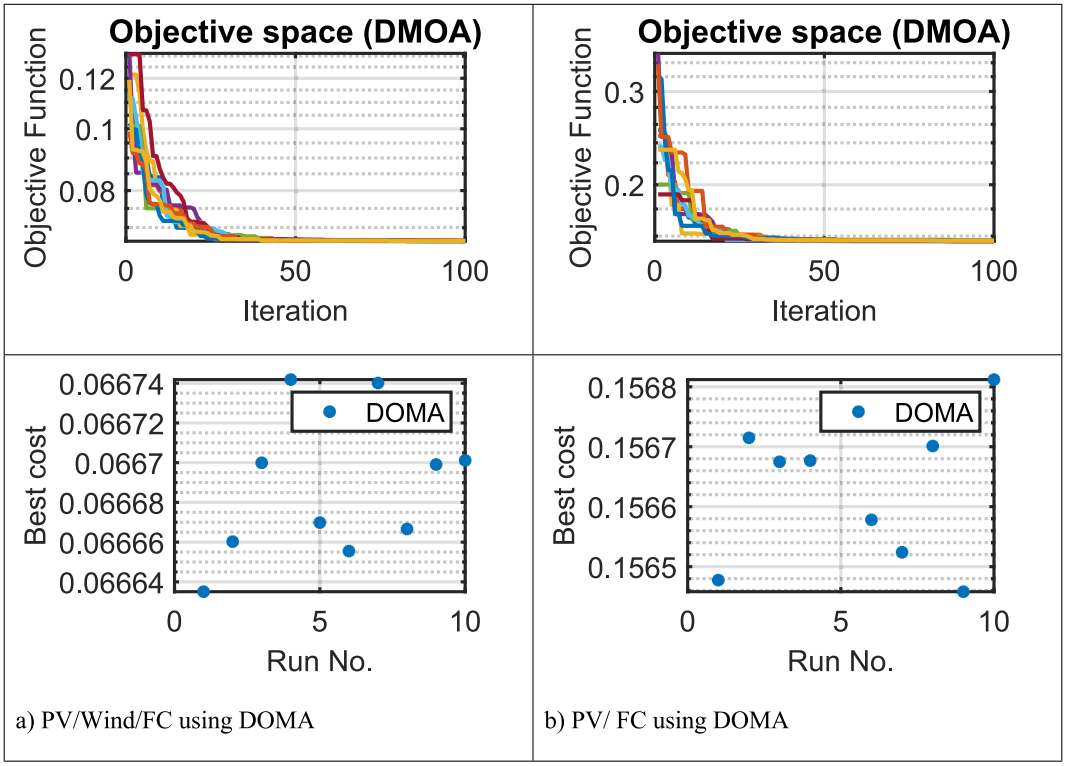

Fig. 15. The results of 10 individual runs using using DOMA: a) PV/Wind/FC using DOMA and b) PV/ FC using DOMA.

Table 6
Comparative performance metrics of the PV/Wind/FC and PV/FC hybrid energy systems optimized using WOA, DOMA, and the proposed MSA.

Metric	PV/Wind/FC using WOA	PV/Wind/FC using DOMA	PV/Wind/FC using MSA	PV/ FC using WOA	PV/ FC using DOMA	PV/ FC using MSA
Mean Cost	0.0685	0.066687	0.0666	0.1589	0.156637	0.1564
Median Cost	0.0680	0.066684	0.0666	0.1587	0.156676	0.1564
Minimum Cost	0.0673	0.066635	0.0666	0.1567	0.156458	0.1564
Worst (Max) Cost	0.0714	0.066742	0.0666	0.1626	0.156812	0.1564
Standard Deviation (SD)	0.1345	0.003568	5.5039e-06	0.1572	0.01203	5.6091e-06
Relative Error (RE)	0.1749	0.007786	1.1993e-05	0.1382	0.011411	4.4793e-06
Mean Absolute Error (MAE)	0.0012	5.19E-05	7.9850e-08	0.0022	0.000179	7.0050e-08
Root Mean Square Error (RMSE)	0.0017	6.19E-05	9.5407e-08	0.0026	0.000212	8.7969e-08
Efficiency (%)	98.3147	99.92223	99.9999	98.6456	99.88608	100.0000
Wilcoxon Signed Rank p-value	0.0020	0.001953	0.0020	0.0020	0.001953	0.0020
Hypothesis Test Result (h)	1 (Significant)	1 (Significant)	1 (Significant)	1 (Significant)	1 (Significant)	1 (Significant)

indicates improved optimization performance and possibly better energy management compared to the PV/FC configuration.

Moreover, the Wilcoxon Signed-Rank Test has been performed for the application of the MSA for optimizing the two systems. The p-value is 0.0020 and the h (hypothesis result) is 1 (significant). This non-parametric test confirms a statistically significant difference between the two configurations at the 5 % level, since $p < 0.05$ and $h = 1$.

5.4. Sensitivity analysis

Sensitivity analysis has been performed to show the impact of the changes in the number of renewable sources—specifically PV panels and wind turbines in the performance of a smart grid system. By keeping the electrolyzer, FC, and hydrogen Tank fixed at their optimal values, the effect of renewable components has been considered on key metrics such as total cost, cost of energy (COE), loss of power supply probability (LPSP), and dummy load.

The results show that increasing the number of PV panels and wind turbines from zero to a level that meets the load generally increases total cost and COE during the search for optimal sizing, as shown in Fig. 9 for PV/Wind/FC configuration. While total cost eventually declines with more renewables, the rate of improvement drops after a certain point. This indicates an optimal capacity beyond which additional units offer minimal economic gain. As more PV panels and wind turbines are added, LPSP decreases sharply. This means the system becomes more reliable and better at meeting demand. LPSP is a key measure of reliability: a value of zero or less means the system fully meets the load, while a positive value signals a shortfall. Dummy load values fluctuate with renewable output, highlighting the variability of these sources. This supports the need for energy storage to smooth out fluctuations. Overall, the analysis confirms that finding the right mix and number of renewable sources is essential to balance cost and reliability. Fig. 10 presents the sensitivity analysis of the PV/Wind/FC configuration, focusing on variations in electrolyzer and fuel cell (FC) power while keeping other components fixed. The results indicate that increasing the power of both the FC and electrolyzer leads to a rise in system costs.

However, advancements in technology and the future development of more efficient and cost-effective FCs and electrolyzers could significantly enhance the reliability of the microgrid. Reduced costs for these components would improve economic feasibility while maintaining system stability and performance. The results are also performed for the second configuration of PV/FC configuration. Fig. 11 shows the sensitivity analysis considering the variation in the electrolyzer and FC power at fixed values of other components for PV/FC configuration.

5.5. Break-even grid extension distance

The Break-Even Grid Extension Distance (BED) is an effective indicator for selecting installations situated at a considerable distance from the grid [35]. BED aims to illustrate the cost-effectiveness of off-grid hybrid energy solutions in comparison to grid extension [60]. The BED can be calculated using the subsequent expression [61]:

$$D_{grid} = \frac{NPC_{off\text{-}grid} \times CRF - COE_{grid} \times AL}{Cost_{grid} \times CRF + O\&M_{grid}}$$

The break-even grid extension distance is denoted as D_{grid} (km), the net present cost of the stand-alone system is indicated by $NPC_{off\text{-}grid}$ ($), the cost of purchasing power from the grid is represented by COE_{grid} $\left(\frac{\$}{kWh}\right)$, the total investment cost for grid expansion is denoted as $Cost_{grid}$ ($/km), the annual operating and maintenance expenses for the grid extension are represented by $O\&M_{grid}$ ($/km/year), the total annual load demand is indicated by AL ($\frac{kWh}{year}$), and the capital recovery factor is represented by CRF. The total projected cost for investment, operation, and maintenance of the grid extension was estimated at $14,000 and $300 per kWh year, correspondingly. Considering the geography of the location implies that in geographically challenging areas, where grid expansion is difficult and costly. In KSA, power costs differ by user category: high-energy customers are charged $0.17/kWh, medium-energy consumers $0.15/kWh, and low-energy consumers $0.09/kWh. In the paper, it has been considered $0/15/kWh. This research examined the specified hybrid systems for each of the three consumer categories.

The BED for the PV/FC system varies significantly across cases, ranging from 376.41 km (Case 2) to 572.14 km (Case 3) as shown in Fig. 12. Cases 1 and 3 have the highest BED values, around 572 km, indicating that off-grid solutions remain cost-effective over long distances. Case 4 falls in between at 513.84 km, while Case 2 has the lowest BED, suggesting that grid extension becomes viable at a much shorter distance. These variations highlight the impact of system costs, energy demand, and operational expenses on the economic feasibility of off-grid versus grid-connected solutions.

The BED for the PV/Wind/FC system varies significantly across cases, ranging from 18.21 km (Case 2) to 143.66 km (Case 4). Cases 1 and 4 have the highest BED values, around 143 km, indicating that off-grid solutions are cost-effective for relatively long distances. In contrast, Case 2 has the lowest BED, suggesting that grid extension is the more economical option for shorter distances. Case 3, with a BED of 40.72 km, falls between these extremes. The substantial differences in BED across cases show the influence of system costs, energy demand, and grid electricity pricing on the economic feasibility of off-grid hybrid energy solutions. The results of such a case study are shown in Fig. 13.

A higher BED means that the grid extension is less economically viable, making the off-grid system more cost-effective for longer distances. The PV/Wind/FC system, with a lower BED (18.21–143.66 km), is more economically competitive in off-grid scenarios compared to the PV/FC system, which has a higher BED (376.41–572.14 km). This suggests that integrating wind power improves the cost-effectiveness of off-grid solutions, reducing reliance on grid extension.

5.6. Algorithm comparison and justification

In accordance with the No Free Lunch (NFL) theorem, which states that no optimization algorithm performs best across all problem types, a comparative analysis was conducted using two well-known algorithms alongside the proposed MSA. This comparison aims to validate the robustness and effectiveness of MSA under the same problem settings. The first is the Whale Optimization Algorithm (WOA) [62], a widely recognized and established benchmark optimization algorithm. The second is the Dwarf Mongoose Optimization Algorithm (DMOA) [63], a recent method known for its efficiency and adaptability.

Both algorithms were applied to optimize the PV/Wind/FC and PV/FC off-grid hybrid energy systems under Case 1–Config 1 and Case 1–Config 2 scenarios. The optimal results obtained are summarized in Table 5. This comparison aims to evaluate the performance, robustness, and applicability of the proposed solution under different algorithmic strategies. The results motivate the strengths and trade-offs of each method, offering valuable insights for selecting appropriate algorithms in future system designs.

Figs. 14 and 15 present the optimization consistency across 10 independent runs for both system configurations using WOA and DOMA. Fig. 14 shows the results using WOA for (a) PV/Wind/FC and (b) PV/FC systems. Fig. 15 illustrates the outcomes using DOMA for the same configurations.

Table 5 presents the comparative performance of two hybrid energy system configurations—PV/Wind/FC and PV/FC—each optimized using three different algorithms: WOA, DOMA, and the proposed Modified MSA. The PV/Wind/FC system optimized with MSA achieved the lowest Loss of Power Supply Probability (LPSP) at 0.02257 and a moderate Cost of Energy (COE) of 0.2375 \$/kWh, showing a balanced trade-off between reliability and cost. The same configuration under DOMA yielded the lowest LPSP at 0.02215 but at a slightly higher COE of 0.2410. WOA resulted in a marginally higher COE and LPSP. In terms of system components, the MSA required 557 PV units, 119 wind turbines, a 734.6 kW electrolyzer, a 257.9 kg maximum hydrogen tank, and a 130.6 kW fuel cell.

In contrast, the PV/FC configuration, which excludes wind turbines, showed significantly higher COE and dumped energy (P_dum) across all algorithms. For instance, MSA produced a COE of 0.5003 and P_dum of 0.7677, both higher than their counterparts in the PV/Wind/FC configuration. The number of required PV panels was also substantially larger, with MSA needing 3465 units. Moreover, the fuel cell rating and tank size were much larger in this configuration, indicating increased system size and cost to maintain reliability in the absence of wind generation. Overall, the PV/Wind/FC system optimized using MSA offers the best balance between cost, reliability, and component sizing among all evaluated configurations and algorithms.

Despite the promising and competitive results achieved by the MSA, it suffers from a major drawback in terms of computational efficiency. The execution time of MSA for both system configurations (PV/Wind/FC and PV/FC) is significantly higher than that of the WOA and the DOMA. Although MSA yielded strong optimization results, the longer runtime limits its practical deployment in time-sensitive or real-time applications. This trade-off must be considered when selecting an algorithm for hybrid renewable system design.

Table 6 presents the comparative performance metrics for the PV/Wind/FC and PV/FC off-grid hybrid energy systems optimized using three algorithms: WOA, DOMA, and the proposed MSA. The results clearly demonstrate the strong performance of MSA across both system configurations. It achieved the lowest mean, median, and worst-case costs, indicating better convergence behavior. MSA also recorded the smallest standard deviation, reflecting consistent and stable outcomes across multiple runs. In terms of error metrics, MSA outperformed WOA and DOMA with the lowest relative error, MAE, and RMSE values, confirming its superior accuracy. Additionally, it reached nearly 100 % efficiency in both system types. Although all algorithms passed the

Wilcoxon signed-rank test with statistically significant results ($p < 0.05$, $h = 1$), MSA exhibited the tightest performance spread and highest reliability. These results validate MSA as a robust and precise optimizer for hybrid renewable energy system design.

5.7. Assumptions, and limitations

The modeling and optimization of the off-grid system rely on assumptions to simplify the analysis while maintaining computational efficiency. It is assumed that all system components operate under steady-state conditions without performance degradation over time. The efficiencies of photovoltaic panels, wind turbines, fuel cells, and electrolyzers are considered constant, neglecting potential variations due to aging or environmental factors. While employing a curve model for fitting purposes allows for a more precise representation of the turbine's actual performance, especially in regions with frequent wind speed variations, the cubic power curve model is assumed to be used for wind turbine simulation in this study. Moreover, the wind speed impact on the outpower of the PV has been neglected. The system is modeled to function under actual weather and load conditions without unexpected failures or downtimes. Additionally, hydrogen storage losses are assumed to be negligible, ensuring that all produced hydrogen remains available for conversion. Economic parameters, such as the discount rate and inflation, are considered constant throughout the system's lifetime, which may not reflect real-world financial fluctuations. Additionally, the study is specific to the Najran region, where climatic conditions favor high solar and wind potential. The results may not be directly applicable to other regions with different renewable resource availability. Uncertainties in the model primarily stem from variability in solar radiation and wind speed, which directly affect energy production and system reliability. Additionally, the convergence behavior of the mantis search algorithm (MSA) depends on parameter tuning and initialization, potentially influencing optimization results. Economic uncertainties, including changes in equipment costs, maintenance expenses, and fuel cell efficiency over time, could alter the financial viability of the proposed system. These uncertainties highlight the need for sensitivity analysis to assess the robustness of the results under different conditions.

6. Conclusion

This paper investigates the optimal design and configuration of a hybrid power system that is dependent on the load demand in Najran, KSA. The proposed hybrid system integrates PV, wind farms, and fuel cell-generating systems. The optimization program is applied to two configurations of the hybrid system: one without wind power plants and the other with wind power plants. Employing the MSA optimization technique, the optimal sizing for both configurations is conducted with the aim of covering the load demand at the lowest COE, maintaining an acceptable reliability index, minimizing fluctuation in the energy supplied to the external grid, and maximizing the utilization of available renewable resources in the region. This study thoroughly analyzes the results obtained from three different configurations. The results indicate that the PV/Wind/FC configuration outperforms the PV/FC system in terms of both COE and LPSP, demonstrating more efficient energy production and greater reliability across all four cases. Specifically, for the PV/Wind/FC system, COE values range from 0.161154 US$/kWh (Case 2-Config 1) to 0.237477 US$/kWh (Case 1-Config 1), and LPSP ranges from 0.022517 % (Case 4-Config 1) to 0.057322 % (Case 2-Config 1). In comparison, the PV/FC system exhibits higher COE values from 0.380493 US$/kWh (Case 2-Config 2) to 0.500352 US$/kWh (Case 3-Config 2), and LPSP values ranging from 0.036985 % (Case 1-Config 2) to 0.099117 % (Case 2-Config 2). These findings highlight the PV/Wind/FC system as a more cost-effective and reliable solution, particularly in scenarios where minimizing energy costs and ensuring high reliability are critical. The Break-Even Grid Extension Distance analysis indicates that the PV/Wind/FC system is more suitable for off-grid deployment in areas with shorter grid extension distances, while the PV/FC system becomes increasingly advantageous as the distance to the grid exceeds 376 km, highlighting its effectiveness for longer-distance scenarios.

Future work will extend the analysis using a full-year dataset to evaluate model robustness under seasonal variability. Additional directions include integrating hybrid storage systems, modeling uncertainty in renewable generation and load, and applying real-time control with demand-side management. System performance will be assessed in terms of cost, reliability, and environmental impact, including secondary hydrogen storage optimization. Advanced optimization methods will be explored to improve scalability. The framework will be enhanced by incorporating recent machine learning algorithms for forecasting, control, and energy management. Long-term benefits of improved forecasting accuracy will be quantified by simulating its effect on dispatch, curtailment, and operational cost, requiring integration with real-time control systems.

CRediT authorship contribution statement

Saleh Awadh AL Dawsari: Writing – original draft, Software, Resources, Methodology, Investigation, Formal analysis, Data curation, Conceptualization. **Fatih Anayi:** Writing – review & editing, Supervision, Project administration, Methodology, Formal analysis, Data curation. **Michael Packianather:** Writing – review & editing, Supervision, Software.

Declaration of competing interest

The authors declare that they have no known competing financial interests or personal relationships that could have appeared to influence the work reported in this paper.

Data availability

The data that has been used is confidential.

References

[1] E. M. Sayed, K. H. Ibrahiem, A. Farhan, and M. M. Samy, "Feasibility Analysis and Techno-Economic Study for Green Energy System Connected to Unhealthy Grid," in *2024 25th International Middle East Power System Conference (MEPCON)*, IEEE, Dec. 2024, pp. 1–6. doi: 10.1109/MEPCON63025.2024.10850253.

[2] A. Fatih Guven, A. Y. Abdelaziz, M. Mahmoud Samy, and S. Barakat, "Optimizing energy Dynamics: A comprehensive analysis of hybrid energy storage systems integrating battery banks and supercapacitors," *Energy Convers Manag*, vol. 312, p. 118560, Jul. 2024, doi: 10.1016/j.enconman.2024.118560.

[3] Das S, De S, Dutta R, De S. Multi-criteria decision-making for techno-economic and environmentally sustainable decentralized hybrid power and green hydrogen cogeneration system. Renew Sustain Energy Rev Mar. 2024;191:114135. https://doi.org/10.1016/j.rser.2023.114135.

[4] H. M. Sultan, A. S. Menesy, and A. A. Zaki Diab, "Algorithms for techno-economic assessment of configuration and size of renewable energy systems," in *Power Systems and Smart Grids. Volume 1*, United Kingdom: The Institution of Engineering and Technology, 2024, pp. 147–177. doi: 10.1049/PBPO264F_ch4.

[5] Y. W. Koholé, C. A. Wankouo Ngouleu, F. C. V. Fohagui, and G. Tchuen, "Optimization and comparative analysis of hybrid renewable energy systems for sustainable and clean energy production in rural Cameroon considering the loss of power supply probability concept," *Energy Conversion and Management: X*, vol. 25, p. 100829, Jan. 2025, doi: 10.1016/j.ecmx.2024.100829.

[6] Diab AAZ, El-Rifaie AM, Zaky MM, Tolba MA. Optimal sizing of stand-alone microgrids based on recent metaheuristic algorithms. Mathematics Jan. 2022;10 (1):140. https://doi.org/10.3390/math10010140.

[7] A. A. Z. Diab, I. Y. Fawzy, A. M. Elsawy, and A. G. Abo El-Magd, "Enhancing Voltage Stability in PV/Wind Power Systems with STATCOM Utilizing Fuzzy Controller," *Journal of Engineering Advances and Technologies for Sustainable Applications*, vol. 1, no. 2, pp. 32–53, Apr. 2025, doi: 10.21608/jeatsa.2025.427967.

[8] Y. W. Koholé, F. C. V. Fohagui, C. A. Wankouo Ngouleu, and G. Tchuen, "An effective sizing and sensitivity analysis of a hybrid renewable energy system for household, multi-media and rural healthcare centres power supply: A case study of Kaele, Cameroon," *Int J Hydrogen Energy*, vol. 49, pp. 1321–1359, Jan. 2024, doi: 10.1016/j.ijhydene.2023.09.093.

[9] Sun X, He H, Ma L. Harmony search meta-heuristic algorithm based on the optimal sizing of wind-battery hybrid micro-grid power system with different battery technologies. J Energy Storage Jan. 2024;75:109582. https://doi.org/10.1016/j.est.2023.109582.

[10] H. J. El-Khozondar, F. El-Batta, R. J. El-Khozondar, Y. Nassar, M. Alramlawi, and S. Alsadi, "Standalone hybrid PV/wind/diesel-electric generator system for a COVID-19 quarantine center," *Environ Prog Sustain Energy*, pp. e14049–e14049, Dec. 2022, doi: 10.1002/ep.14049.

[11] C. A. Wankouo Ngouleu, Y. W. Koholé, F. C. V. Fohagui, and G. Tchuen, "Techno-economic analysis and optimal sizing of a battery-based and hydrogen-based standalone photovoltaic/wind hybrid system for rural electrification in Cameroon based on meta-heuristic techniques," *Energy Convers Manag*, vol. 280, p. 116794, Mar. 2023, doi: 10.1016/j.enconman.2023.116794.

[12] H. M. Sultan, M. A. Mossa, A. A. Zaki Diab, and N. El Ouanjli, "Enhanced Techno-Economical Optimal Sizing of a Standalone Hybrid Microgrid Power System," 2025, pp. 107–138. doi: 10.1007/978-981-96-2665-6_6.

[13] O. Makram Kamel, I. Elzein, M. M. Mahmoud, A. Y. Abdelaziz, M. M. Hussein, and A. A. Zaki Diab, "Effective energy management strategy with a novel design of fuzzy logic and JAYA-based controllers in isolated DC/AC microgrids: A comparative analysis," *Wind Engineering*, vol. 49, no. 1, pp. 199–222, Feb. 2025, doi: 10.1177/0309524X241263518.

[14] M. M. Torad, S. H. A. Elbanna, M. A. El-Dabah, and A. A. Z. Diab, "Optimal Design of a Grid-Connected Microgrid Incorporating Biomass: Case Study in New Valley, Egypt," in *2025 7th International Youth Conference on Radio Electronics, Electrical and Power Engineering (REEPE)*, IEEE, Apr. 2025, pp. 1–8. doi: 10.1109/REEPE63962.2025.10971032.

[15] Khosravi N, Oubelaid A, Belkhier Y. Energy management in networked microgrids: a comparative study of hierarchical deep learning and predictive analytics techniques. Energy Convers Manage: X Jan. 2025;25:100828. https://doi.org/10.1016/j.ecmx.2024.100828.

[16] Khan A, Javaid N. Optimal sizing of a stand-alone photovoltaic, wind turbine and fuel cell systems. Comput Electr Eng Jul. 2020;85. https://doi.org/10.1016/j.compeleceng.2020.106682.

[17] Ahmad J, et al. Techno economic analysis of a wind-photovoltaic-biomass hybrid renewable energy system for rural electrification: a case study of Kallar Kahar. Energy Apr. 2018;148:208–34. https://doi.org/10.1016/j.energy.2018.01.133.

[18] Beza TM, Wu CH, Kuo CC. Optimal sizing and techno-economic analysis of minigrid hybrid renewable energy system for tourist destination islands of lake tana, ethiopia. Appl Sci (Switzerland) 2021;11(15):Aug. https://doi.org/10.3390/app11157085.

[19] El Shamy AR, Aduama P, Al-Sumaiti AS. Chance constrained optimal sizing of a hybrid PV/battery/hydrogen isolated microgrid: a life-cycle analysis. Energy Convers Manag May 2025;332:119707. https://doi.org/10.1016/j.enconman.2025.119707.

[20] Md. F. Ali, Md. R. Islam Sheikh, M. Md. Julhash, and A. H. Sanvi, "Sustainable electrification of remote communities: Techno-economic and demand response analysis for renewable microgrids," *Energy Conversion and Management: X*, vol. 26, p. 100963, Apr. 2025, doi: 10.1016/j.ecmx.2025.100963.

[21] R. Siddaiah and R. P. Saini, "A review on planning, configurations, modeling and optimization techniques of hybrid renewable energy systems for off grid applications," May 01, 2016, *Elsevier Ltd*. doi: 10.1016/j.rser.2015.12.281.

[22] Alshammari NF, Samy MM, Barakat S. Comprehensive analysis of multi-objective optimization algorithms for sustainable hybrid electric vehicle charging systems. Mathematics Apr. 2023;11(7):1741. https://doi.org/10.3390/math11071741.

[23] Tazay AF, Samy MM, Barakat S. A techno-economic feasibility analysis of an autonomous hybrid renewable energy sources for university building at Saudi Arabia. J Elec Eng Technol 2020;15(6):2519–27. https://doi.org/10.1007/s42835-020-00539-x.

[24] M. Vaccari, G. M. Mancuso, J. Riccardi, M. Cantù, and G. Pannocchia, "A Sequential Linear Programming algorithm for economic optimization of Hybrid Renewable Energy Systems," *J Process Control*, pp. 189–201, Feb. 2019, doi: 10.1016/j.jprocont.2017.08.015.

[25] Alberizzi JC, Frigola JM, Rossi M, Renzi M. Optimal sizing of a Hybrid Renewable Energy System: Importance of data selection with highly variable renewable energy sources. Energy Convers Manag Nov. 2020;223. https://doi.org/10.1016/j.enconman.2020.113303.

[26] Singh P, Pandit M, Srivastava L. Multi-objective optimal sizing of hybrid micro-grid system using an integrated intelligent technique. Energy Apr. 2023;269. https://doi.org/10.1016/j.energy.2023.126756.

[27] Samy MM, Mosaad MI, El-Naggar MF, Barakat S. Reliability support of undependable grid using green energy systems: economic study. IEEE Access 2021;9:14528–39. https://doi.org/10.1109/access.2020.3048487.

[28] Mokhtara C, Negrou B, Settou N, Settou B, Samy MM. Design optimization of off-grid hybrid renewable energy systems considering the effects of building energy performance and climate change: Case study of Algeria. Energy 2021;219:119605. https://doi.org/10.1016/j.energy.2020.119605.

[29] Javed MS, Ma T, Jurasz J, Ahmed S, Mikulik J. Performance comparison of heuristic algorithms for optimization of hybrid off-grid renewable energy systems. Energy Nov. 2020;210. https://doi.org/10.1016/j.energy.2020.118599.

[30] Fathy A, Kaaniche K, Alanazi TM. Recent approach based social spider optimizer for optimal sizing of hybrid PV/Wind/battery/diesel integrated microgrid in aljouf region. IEEE Access 2020;8:57630–45. https://doi.org/10.1109/ACCESS.2020.2982805.

[31] Kumar PP, Saini RP. Optimization of an off-grid integrated hybrid renewable energy system with different battery technologies for rural electrification in India. J Energy Storage Dec. 2020;32. https://doi.org/10.1016/j.est.2020.101912.

[32] Thirunavukkarasu M, Sawle Y, Lala H. A comprehensive review on optimization of hybrid renewable energy systems using various optimization techniques. Renew Sustain Energy Rev Apr. 2023;176:113192. https://doi.org/10.1016/j.rser.2023.113192.

[33] Giedraityte A, Rimkevicius S, Marciukaitis M, Radziukynas V, Bakas R. Hybrid renewable energy systems—A review of optimization approaches and future challenges. Appl Sci Feb. 2025;15(4):1744. https://doi.org/10.3390/app15041744.

[34] Saini K, Saini M, Kumar A, Saini DK. Performance analysis and optimization in renewable energy systems: a bibliometric review. Discover Appl Sci Feb. 2025;7(3):178. https://doi.org/10.1007/s42452-025-06585-2.

[35] Y. W. Koholé, C. A. Wankouo Ngouleu, F. C. V. Fohagui, and G. Tchuen, "A comprehensive comparison of battery, hydrogen, pumped-hydro and thermal energy storage technologies for hybrid renewable energy systems integration," *J Energy Storage*, vol. 93, p. 112299, Jul. 2024, doi: 10.1016/j.est.2024.112299.

[36] Y. W. Koholé, C. A. Wankouo Ngouleu, F. C. V. Fohagui, and G. Tchuen, "Optimization of an off-grid hybrid photovoltaic/wind/diesel/fuel cell system for residential applications power generation employing evolutionary algorithms," *Renew Energy*, vol. 224, p. 120131, Apr. 2024, doi: 10.1016/j.renene.2024.120131.

[37] Y. W. Koholé, B. R. Ngopgang, F. C. V. Fohagui, C. A. Wankouo Ngouleu, and G. Tchuen, "Green hydrogen production and storage via excess energy derived from a hybrid power system under different climatic conditions: Cameroon case study," *Energy Convers Manag*, vol. 325, p. 119418, Feb. 2025, doi: 10.1016/j.enconman.2024.119418.

[38] Koholé YW, Fohagui FCV, Djiela RHT, Tchuen G. Wind energy potential assessment for co-generation of electricity and hydrogen in the far North region of Cameroon. Energy Convers Manag Mar. 2023;279:116765. https://doi.org/10.1016/j.enconman.2023.116765.

[39] Y. W. Koholé, C. A. Wankouo Ngouleu, F. C. V. Fohagui, and G. Tchuen, "Quantitative techno-economic comparison of a photovoltaic/wind hybrid power system with different energy storage technologies for electrification of three remote areas in Cameroon using Cuckoo search algorithm," *J Energy Storage*, vol. 68, p. 107783, Sep. 2023, doi: 10.1016/j.est.2023.107783.

[40] C. A. Wankouo Ngouleu, Y. W. Koholé, F. C. V. Fohagui, and G. Tchuen, "Optimum design and scheduling strategy of an off-grid hybrid photovoltaic-wind-diesel system with an electrochemical, mechanical, chemical and thermal energy storage systems: A comparative scrutiny," *Appl Energy*, vol. 377, p. 124646, Jan. 2025, doi: 10.1016/j.apenergy.2024.124646.

[41] C. A. Wankouo Ngouleu, Y. W. Koholé, F. C. V. Fohagui, and G. Tchuen, "Optimal sizing and techno-enviro-economic evaluation of a hybrid photovoltaic/wind/diesel system with battery and fuel cell storage devices under different climatic conditions in Cameroon," *J Clean Prod*, vol. 423, p. 138753, Oct. 2023, doi: 10.1016/j.jclepro.2023.138753.

[42] Nasser M, Megahed TF, Ookawara S, Hassan H. Techno-economic assessment of clean hydrogen production and storage using hybrid renewable energy system of PV/Wind under different climatic conditions. Sustain Energy Technol Assess Aug. 2022;52:102195. https://doi.org/10.1016/j.seta.2022.102195.

[43] Ourya I, Nabil N, Abderafi S, Boutammachte N, Rachidi S. Assessment of green hydrogen production in Morocco, using hybrid renewable sources (PV and wind). Int J Hydrogen Energy Dec. 2023;48(96):37428–42. https://doi.org/10.1016/j.ijhydene.2022.12.362.

[44] Zhu M, Xiang D, Cao H, Liu L, Guo C. Techno-economic analysis of green hydrogen production using a 100 MW photovoltaic power generation system for five cities in North and Northwest China. Sol Energy Feb. 2024;269:112312. https://doi.org/10.1016/j.solener.2024.112312.

[45] Martire M, Kaya AF, Morselli N, Puglia M, Allesina G, Pedrazzi S. Analysis and optimization of a hybrid system for the production and use of green hydrogen as fuel for a commercial boiler. Int J Hydrogen Energy Feb. 2024;56:769–79. https://doi.org/10.1016/j.ijhydene.2023.12.223.

[46] O. W. Khalid, N. A. M. Isa, and H. A. Mat Sakim, "Emperor penguin optimizer: A comprehensive review based on state-of-the-art meta-heuristic algorithms," *Alexandria Engineering Journal*, vol. 63, pp. 487–526, Jan. 2023, doi: 10.1016/j.aej.2022.08.013.

[47] Zhou J, Xu Z. Optimal sizing design and integrated cost-benefit assessment of stand-alone microgrid system with different energy storage employing chameleon swarm algorithm: a rural case in Northeast China. Renew Energy Jan. 2023;202:1110–37. https://doi.org/10.1016/j.renene.2022.12.005.

[48] Ashraf MA, Liu Z, Alizadeh A, Nojavan S, Jermsittiparsert K, Zhang D. Designing an optimized configuration for a hybrid PV/Diesel/Battery Energy System based on metaheuristics: a case study on Gobi Desert. J Clean Prod Oct. 2020;270. https://doi.org/10.1016/j.jclepro.2020.122467.

[49] Mohammadi M, Hosseinian SH, Gharehpetian GB. Optimization of hybrid solar energy sources/wind turbine systems integrated to utility grids as microgrid (MG) under pool/bilateral/hybrid electricity market using PSO. Sol Energy Jan. 2012;86(1):112–25. https://doi.org/10.1016/j.solener.2011.09.011.

[50] Nelson DB, Nehrir MH, Wang C. Unit sizing and cost analysis of stand-alone hybrid wind/PV/fuel cell power generation systems. Renew Energy Aug. 2006;31(10):1641–56. https://doi.org/10.1016/j.renene.2005.08.031.

[51] Maleki A, Askarzadeh A. Artificial bee swarm optimization for optimum sizing of a stand-alone PV/WT/FC hybrid system considering LPSP concept. Sol Energy 2014;107:227–35. https://doi.org/10.1016/j.solener.2014.05.016.

[52] Sultan HM, Menesy AS, Kamel S, Korashy A, Almohaimeed SA, Abdel-Akher M. An improved artificial ecosystem optimization algorithm for optimal configuration of a hybrid PV/WT/FC energy system. Alex Eng J Feb. 2021;60(1):1001–25. https://doi.org/10.1016/j.aej.2020.10.027.

[53] Garcia RS, Weisser D. A wind-diesel system with hydrogen storage: Joint optimisation of design and dispatch. Renew Energy Nov. 2006;31(14):2296–320. https://doi.org/10.1016/j.renene.2005.11.003.
[54] Ramli MAM, Bouchekara HREH, Alghamdi AS. Optimal sizing of PV/wind/diesel hybrid microgrid system using multi-objective self-adaptive differential evolution algorithm. Renew Energy Jun. 2018;121:400–11. https://doi.org/10.1016/j.renene.2018.01.058.
[55] A. A. Z. Diab, S. I., H. M., and Y. B., "Modified Farmland Fertility Optimization Algorithm for Optimal Design of a Grid-connected Hybrid Renewable Energy System with Fuel Cell Storage: Case Study of Ataka, Egypt," *International Journal of Advanced Computer Science and Applications*, vol. 10, no. 8, 2019, doi: 10.14569/ijacsa.2019.0100817.
[56] Sultan HM, Menesy AS, Kamel S, Korashy A, Almohaimeed SA, Abdel-Akher M. An improved artificial ecosystem optimization algorithm for optimal configuration of a hybrid PV/WT/FC energy system. Alex Eng J 2021;60(1):1001–25.
[57] Abdel-Basset M, Mohamed R, Zidan M, Jameel M, Abouhawwash M. Mantis Search Algorithm: a novel bio-inspired algorithm for global optimization and engineering design problems. Comput Methods Appl Mech Eng 2023;415:116200.
[58] Raza A, Chen Y, Li M, Abouzeid SI, Abdelhameed EH. Feasibility and optimal size analysis of off grid hybrid AC-DC microgrid system: Case study of El Kharga Oasis, Egypt. J Energy Storage Sep. 2024;97:112721. https://doi.org/10.1016/j.est.2024.112721.
[59] Aeggegn DB, Nyakoe GN, Wekesa C. Optimal sizing of grid connected multi-microgrid system using grey wolf optimization. Results Eng Sep. 2024;23:102421. https://doi.org/10.1016/j.rineng.2024.102421.
[60] Demirci A, Öztürk Z, Tercan SM. Decision-making between hybrid renewable energy configurations and grid extension in rural areas for different climate zones. Energy Jan. 2023;262:125402. https://doi.org/10.1016/j.energy.2022.125402.
[61] Y. W. Koholé, F. C. V. Fohagui, C. A. Wankouo Ngouleu, and G. Tchuen, "An effective sizing and sensitivity analysis of a hybrid renewable energy system for household, multi-media and rural healthcare centres power supply: A case study of Kaele, Cameroon," *Int J Hydrogen Energy*, vol. 49, pp. 1321–1359, Jan. 2024, doi: 10.1016/j.ijhydene.2023.09.093.
[62] Mirjalili S, Lewis A. The whale optimization algorithm. Adv Eng Softw May 2016;95:51–67. https://doi.org/10.1016/j.advengsoft.2016.01.008.
[63] Agushaka JO, Ezugwu AE, Abualigah L. Dwarf mongoose optimization algorithm. Comput Methods Appl Mech Eng Mar. 2022;391:114570. https://doi.org/10.1016/j.cma.2022.114570.